Estuaries and Coasts (2025) 48:54
https://doi.org/10.1007/s12237-025-01483-7

Dynamics of Yearly Maximum Water Levels in the Amazon Estuary

Paul Coulet[1,2] · Fabien Durand[1,2] · Alice Fassoni-Andrade[2] · Md Jamal Uddin Khan[1] · Laurent Testut[3] · Florence Toublanc[1] · Leandro Guedes Santos[4] · Daniel Medeiros Moreira[5,6] · Alberto Azevedo[7]

Received: 5 May 2023 / Revised: 20 December 2024 / Accepted: 3 January 2025 / Published online: 22 January 2025

Abstract

The magnitude and temporality of the yearly maxima water levels are key parameters for the characterization of the riverine flooding hazard and its impacts. Although the Amazon estuary, that conveys the largest river discharge to the world ocean, exhibits marked events of maxima of the water level every year, the contribution of the natural drivers to these yearly extreme water levels is not well quantified. In this study, we investigate the contributing factors to the yearly maxima water level events along the Amazon estuary using a high-resolution cross-scale hydrodynamic model that has been extensively validated against comprehensive in situ and satellite datasets. Our study shows that the oceanic tide plays a crucial role in the genesis of the yearly maxima, whose influence decays from the downstream part (accounting for 85% of the total water level) towards the upstream part (44% of the total water level) of the estuary. Conversely, the Amazon discharge during the peak flood season induces yearly maxima in the upstream part of the estuary (accounting for 41% of the total water level), but the riverine influence decays sharply towards downstream and remains minor in the region of the mouths (9% of the total water level). Additionally, the sporadic bursts of north-easterly trade winds result in a sizeable wind-setup in the estuary (typically accounting for 5% to 13% of the total water level). Our study underscores the need for considering compound forcing in the cross-scale modeling in Amazon and similar estuaries. At a time when the climatic extremes are becoming more frequent over the Amazon region, our study helps the interpretation of the imprint of these extremes on the water level variability along this estuary.

Keywords Amazon · Sea level · Extreme · Estuary · Tide · Surge

Introduction

Complex estuarine systems and large river deltas around the world stand out as vulnerable territories (Tessler et al., 2015). They are increasingly struck by the coastal floodings and show sensitivity to sea level rise (Edmonds et al., 2020). Yet, they are vital for the economy and food security of many regions worldwide, beyond their own boundaries (Khojasteh et al., 2021; Syvitski et al., 2009). They are also of key importance for the freshwater, sediment, and nutrient budgets of the world ocean, as they are the main conveyors of continental runoff to the oceans (Milliman & Farnsworth, 2011). At the interface of rivers and ocean, they remain relatively less studied than the adjoining coastal ocean or the upstream rivers. Particularly, global flood risk studies focus on either the riverine or the coastal part (Eilander et al., 2020, and references within). The lower part of these mega estuaries typically forms intricate hydraulic systems. The hydrodynamics of these interface zones is indeed complex,

Communicated by David K. Ralston

✉ Fabien Durand
fabien.durand@ird.fr

1 LEGOS, Université Toulouse, IRD, CNRS, CNES, UPS, Toulouse, France

2 Institute of Geosciences, University of Brasília (UnB), Brasília, Brazil

3 LIENSs UMR 7266, CNRS- La Rochelle University, 17000 La Rochelle, France

4 CPRM, Serviço Geológico Do Brasil, Avenida Doutor FreitasMarco, Belém 3645, Brazil

5 CPRM, Serviço Geológico Do Brasil, Avenida Pasteur, Urca, Rio de Janeiro 404, Brazil

6 GET, CNRS/CNES/IRD/UPS, 31400 Toulouse, France

7 Laboratório Nacional de Engenharia Civil (LNEC), Avenida Do Brasil 101, Lisboa, Portugal

under the joint influence of various factors, namely the hydrology of the upstream watershed, the oceanic variability (including the tides, along with swell and wind waves in storm-prone areas), the local atmospheric forcing (viz. the weather), and the dynamic interactions among these. One of the possible reasons for the lack of understanding of their dynamics may be linked to their very broad temporal spectrum of hydraulic variability, with prominent timescales ranging from minutes and hours (typically for the tide and storm surges) to annual, interannual and longer periods (for the seasonal discharge or for the trend of sea level rise for instance). Spatially, the typical braided geometry of the estuarine riverine systems also involves a broad variety of relevant scales, from sub-kilometric channels and creeks to hundreds of kilometers-long tidal rivers reaches for the largest ones. This altogether sets some stringent constraints in any observational or modeling initiative developed to ascertain their dynamics.

The Amazon estuary, the downstream-most fraction of the Amazon River subject to tidal intrusion, is unusual among the estuaries of large rivers worldwide in several ways. It has among the longest tidal reaches, with a macrotidal signal of typical range around 4 m entering the mouths from the Atlantic Ocean, propagating and decaying upstream over more than 800 km inland (Fassoni-Andrade et al., 2023; Kosuth et al., 2009). This energetic tidal signal is favored by the geometry of the Amazon shelf suitable to the resonance of semi-diurnal tides (Beardsley et al., 1995) as well as by the extended fluid mud layer at the Amazon mouth, lowering the dissipation of the tidal energy by bottom friction (Gabioux et al., 2005). The pioneering study of Gallo and Vinzon (2005) has evidenced the role of the M4 overtide and MSf compound tide in the modulation of the tidal signal propagating along the estuary. More recently, Fassoni-Andrade et al. (2023) showed that the upstream limit of the tidal influence varies with the seasonality of the river discharge, ranging from more than 800 km inland in low flow to 500 km inland in high flow.

Gallo and Vinzon (2005) also suggested that the Amazon estuary has a long tidal river (Hoitink & Jay, 2016). Herein, tidal river refers to the section of the tidal reach where the low-tide level of neap tide is lower than the low-tide level of spring tide (Jay et al., 2015). This definition has already been adopted in systems of comparable size such as the Saint Lawrence (Matte et al., 2014) and Yangtze River (Guo et al., 2015).

The Amazon River also conveys the largest discharge of freshwater worldwide (200,000 $m^3.s^{-1}$ on average), accounting for about 20% of the river discharge to the global ocean (Callède et al., 2010). This massive discharge has implications on the regional sea level of the western Atlantic Ocean (Durand et al., 2019). Past studies of Gibbs (1970) and Geyer and Kineke (1995) have evidenced the lack of salt intrusion into the Amazon terminal delta, with a salt front located on the continental shelf, more than 100 km offshore of the river mouths. Amazon River outflows to the Atlantic Ocean on the equator, which has some dynamical implications. The Coriolis force vanishes there; therefore, the riverine freshwater does not get coastally-trapped upon entering the ocean, but rather gets transported offshore by the regional oceanic circulation (Ruault et al., 2020). Although less populated than the Asian deltas of comparable size (such as the Mekong or the Bengal), it is home to 4 million dwellers, as reported in the 2010 census from IBGE (Brazilian Institute of Geography and Statistics) (IBGE, 2010); this population shows swift migratory dynamics, as it has doubled over the past two decades (Szabo et al., 2016). The rapid urbanization in flood-prone areas of the estuary coupled with poor urban infrastructure for domestic water and waste management make a significant part of the riverine population vulnerable and already consistently exposed to flooding hazard (Mansur et al., 2016).

The tidal and river dynamics, vigorous wind forcing (Nikiema et al., 2007), and the extended and shallow Amazon continental shelf (Fassoni-Andrade et al., 2021b), mean that the lower reaches of the Amazon estuary are prone to prominent surges and tide-surge interaction. These interactions can generate extreme sea levels above the tidal high water level (Lyddon et al., 2018a). Regarding the hydrological forcing from the Amazon basin, besides its high magnitude throughout the seasonal cycle, it also exhibits a marked year-to-year variability, with an intensification of the floods reported in the latest decades (Barichivich et al., 2018). Considering the historical records dating back from more than a century ago, it appears that seven of the ten largest floods of the Amazon River have occurred in the past 14 years (2009, 2012, 2013, 2014, 2015, 2019 and 2021; Chevuturi et al., 2021). These floods had distinct impacts on the physics of the western Atlantic Ocean, with far-reaching anomalies of the sea surface salinity (Gévaudan et al., 2022). In a given hydrosystem, compound flooding results from the combination of various independent environmental factors. In the case of the Amazon estuary, the strength of the oceanic tide, of the Amazon discharge, and of the atmospheric forcing altogether point towards their potential role of compounding factors of extreme water level events. Still, to date, the quantitative characterization of these factors of the water level extremes along the estuary remains largely overlooked. Indeed, due to the broad range of timescales at which the previously cited factors act and interact, this remains a complex challenge (Matte et al., 2013). Tides, non-tidal processes, along with their interactions altogether make the spectrum of water level variability nonstationary (Hoitink and Jay, 2016 and references therein).

Various studies have examined tide-river interactions in hydrosystems of comparable size to the Amazon, such as

the Yangtze, the Columbia River, the St Lawrence, and San Francisco Bay (Baranes et al., 2023; Hoitink & Jay, 2016). In particular, the seasonal modulation of the tide induced by tide-discharge interactions has been evidenced in the Yangtze or the Columbia River, through nonstationary harmonic analysis (Guo et al., 2015; Matte et al., 2014).

Considering the non-stationarity of the tide, and the various compounding factors of water level variability, past studies have aimed at hindcasting and forecasting tidal datum levels (e.g., higher high-water level or mean water level) from observational data through regression models (Baranes et al., 2023; Jay et al., 2011). These approaches rely on building robust regression methods based on observational data to analyze the influence of the compounding factors on tidal datum levels. The present study, in contrast, aims to quantify the contribution of each of these factors in the generation of extreme water level events in the Amazon estuary, through comprehensive hydrodynamical modeling.

Studies investigated the along-channel gradient of forcing factors of the water level variations in other estuarine and deltaic contexts although not especially dedicated to the analysis of water level extremes (e.g., Godin (1999) or Matte et al. (2014) over the Saint Lawrence; Guo et al. (2015) over the Yangtze; Sassi et al. (2012) over the Mahakam delta). One such example is the study by Jay et al. (2015) who investigated the dynamics of the Columbia River and estuary. At the mouth of this estuary, the conditions are macrotidal, similarly to the Amazon mouth. They concluded that the transition from tide-dominated regime to river-flow-dominated regime occurs around 100 km upstream of the estuary mouth. In similar tropical estuaries, Hiatt et al. (2019) have emphasized the composite role of river, tide, and atmosphere in coastal water level anomalies, while Khan et al. (2021) demonstrated the pertinence of the use of hydrodynamical models for understanding extreme water level events in such data-scarce hydrosystems. However, to date, no study investigated the specific role of the various compounding forcing factors of the water level extremes over the Amazon estuary. The objective of the present paper is to quantitatively address the dynamics of the yearly water level maxima (hereafter TWLmax) across the estuary, based on a hydrodynamical modeling approach in 2D capable of simulating water level variation from ocean-to-creek scales including wetting and drying of intertidal and intermittently flooded areas. To achieve this, we will hindcast the Amazon estuary dynamics throughout the 2014–2018 period using a nonlinear, cross-scale hydrodynamic model.

The year 2017 is investigated in depth, as it is considered as a year representative of normal conditions as regards to the climatic variability of the Amazon River hydrological cycle. "Data and Methods" presents the modeling framework as well as the in situ water level database used for validation. In "Analysis and Validation of Modeled Water Levels," we provide a thorough validation of the modeled water level variability. "Results: Mechanisms of Water Level Yearly Maximum" describes the mechanisms responsible for the TWLmax occurring across the Amazon estuary, from the upstream region to its oceanic outlet. "Discussion" provides a discussion and conclusion.

Data and Methods

Hydrodynamical Model

For the current work, we have upgraded the configuration of the hydrodynamic model used in Fassoni-Andrade et al. (2023) with extended coverage, higher resolution, revised calibration of the integration timestep, as well as of the spatial distribution of the Manning's coefficient of parameterization of the bottom friction. The model domain spans across the Amazon estuary, from its upstream limit in the region of Óbidos (some 800 km upstream of the mouths), down to the deep Atlantic Ocean (Fig. 1). The model geometry relies on the high-resolution topographic-bathymetric atlas of Fassoni-Andrade et al. (2021b), encompassing the riverine domain as well as the adjoining floodable regions. We used SCHISM, a semi-implicit cross-scale 2D/3D circulation model (Zhang et al., 2016), in depth-integrated mode (2DH). The model domain is discretized in an unstructured computational mesh with 1′039′864 nodes and 2′024′317 triangular elements, with node spacing varying from 5 km in the deep ocean to 40 m in the estuary (Fig. 2). The element size is scaled locally according to both the bathymetry and its gradient, with higher resolution in regions of shallow bathymetry and of steep bathymetric slopes. The limits of the model domain on the deep ocean side are aligned with Topex/Jason spaceborne altimetric tracks, to impose the X-TRACK altimetric tidal constants conditions (XTRACK tidal constants, www.aviso.altimetry.fr/en/data/products/auxiliary-products/coastal-tide-xtrack.html) along these open boundaries. This product is based on the sea level anomaly dataset of the Topex/Poseidon and Jason satellite altimetry mission from 1993 to 2015 with a dedicated processing to improve the quality of the measurement in the coastal zone (Birol et al., 2017). The tidal constituents imposed at the boundary are M2, N2, K2, S2, 2N2, O1, K1, Q1, P1, MF, Mm, M4, MS4, M6, NU2, MU2, T2, SA, SSA, MN4, S1, S4, M3, R2, MSf, and J1. We considered the astronomical tidal forcing over the modeling domain with the tidal potentials of 2N2, K1, K2, L2, M2, MU2, N2, NU2, O1, P1, Q1, S2, and T2. This modeling strategy ensures an accurate modeling of the Atlantic Ocean tide propagating from the deep ocean to the Amazonian oceanic shelf (Fassoni-Andrade et al., 2023). At its upstream limits inland, the model holds open boundaries for the Amazon River

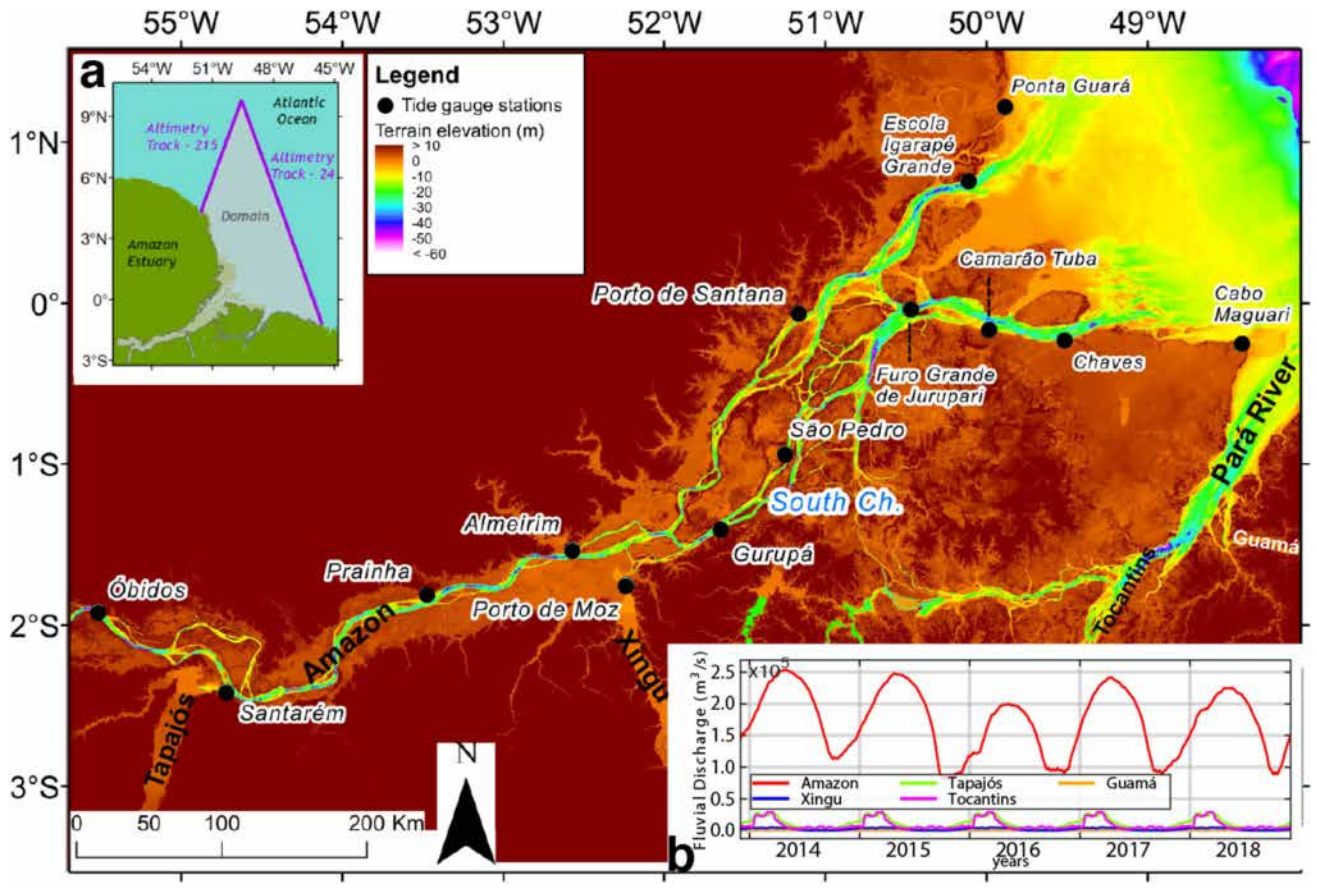

Fig. 1 Bathymetry of the Amazon estuary. The tide gauge stations used subsequently in the study are displayed in blue bullets. Inset (**a**) shows the limits of the modeling domain. Inset (**b**) shows the evolution of the discharge of the various rivers entering the model, over 2014–2018

upstream of Óbidos as well as for all the significant tributaries joining the Amazon downstream of Óbidos (Tapajós River, Xingu River, Tocantins River, and Guamá River). For Amazon and the other rivers, observed discharges were imposed as boundary conditions (ANA, Agência Nacional de Águas, Brazilian water agency, https://www.snirh.gov.br/hidrotelemetria/Estacoes.aspx) (Fig. 1b). The model allows for wetting and drying of all the floodable areas. The reader is referred to Fassoni-Andrade et al. (2023) for further details on the numerics and set-up of the modeling framework. The other differences between Fassoni-Andrade et al. (2023) and the present model set-up are the extension of the domain imprint to the whole Pará River as well as the inclusion of the atmospheric forcing under the form of surface wind and pressure. The wind and pressure fields at the air-sea interface are prescribed at 6-h interval from CFSR version 2 reanalysis (Saha et al., 2011). The model is integrated at a 400-s timestep using a robust semi-implicit scheme with loose constraints on maximum CFL condition.

To investigate the dynamics of water level variability, four different simulations have been carried out, covering the period between 01/11/2013 and 31/12/2018. The forcings of the simulations are summarized in Table 1. The REF simulation considers all forcing fluxes (oceanic tide, rivers discharge, wind, atmospheric pressure), whereas the NOATM simulation does not include any atmospheric forcing (neither wind nor pressure). The NOWIND simulation does not include the wind part of the atmospheric forcing, and the NOPRESS simulation excludes only the pressure part of the atmospheric forcing. For all simulations, the first 2 months (11/2013–12/2013) were discarded to allow for initial spin-up of the model. These sensitivity tests allowed us to compute the various contributing factors to the water level variability, viz. the tide, the river discharge, and the atmosphere. We will focus on assessing the role of these compounding factors on the anomaly of total water level (hereafter TWL) with respect to 2014–2018 climatology. The climatology is computed from NOATM simulation over 2014–2018, which is then smoothed using a 32-day moving window.

We term as "Tidal contribution" (hereafter TIDE), the water level predicted using the dominant tidal constituents (viz. M2, S2, M4, Mm, MSf) (Gallo & Vinzon, 2005). These constituents are obtained every day from the

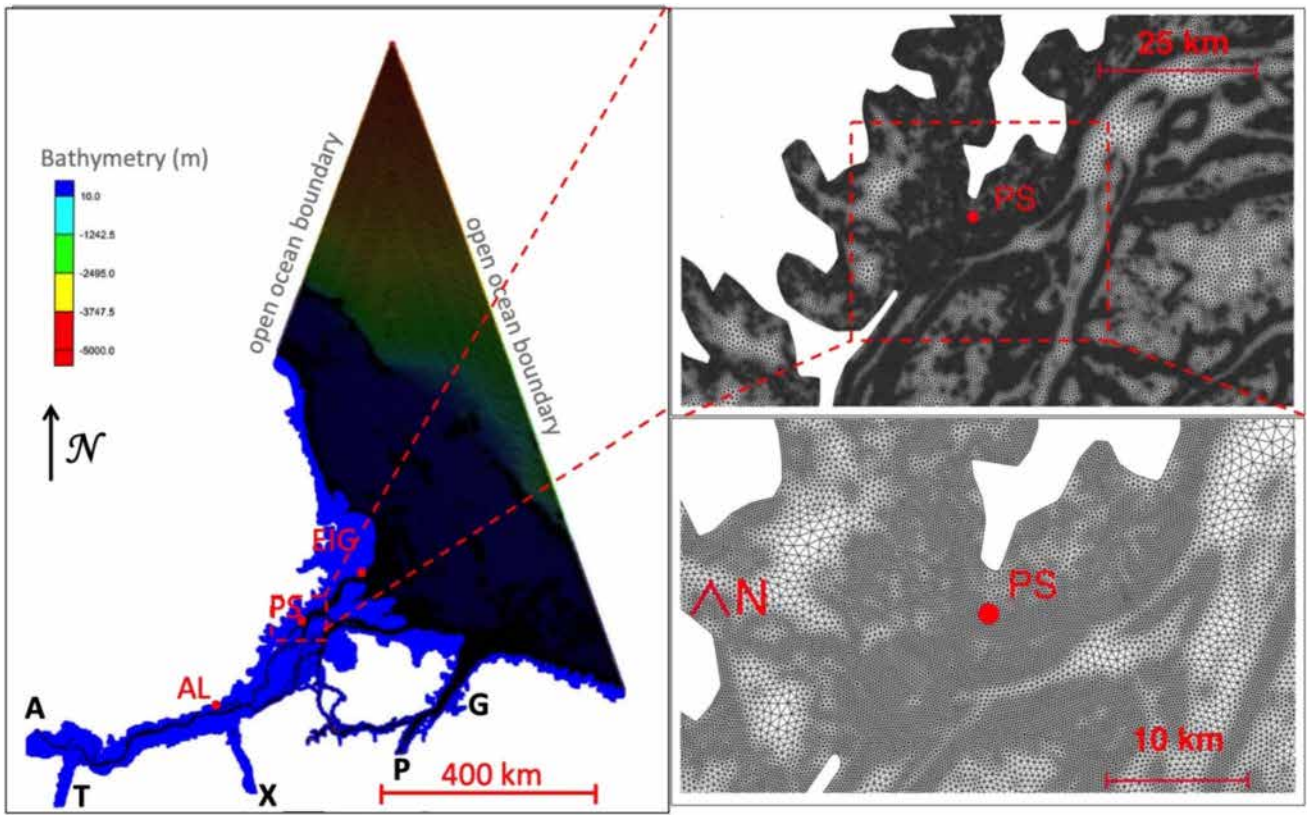

Fig. 2 Model computational unstructured mesh, with zoomed views over the neighborhood of Porto de Santana (labeled PS) in the terminal part of the estuary. AL and EIG stand for Almeirim and Escola do Igarapé Grande, respectively. The locations of the riverine open boundaries are labeled as A (for Amazon), T (for Tapajós), X (for Xingu), P (for Pará), and G (for Guamá)

Table 1 Forcing factors considered in the various modeling experiments carried out, covering the 11/2013–12/2018 period

Simulation name	Tidal forcing	River discharge forcing	Wind forcing	Atmospheric pressure forcing
REF	✓	✓	✓	✓
NOATM	✓	✓		
NOWIND	✓	✓		✓
NOPRESS	✓	✓	✓	

harmonic analysis of 32 days of water level centered on that day using the Python implementation of UTide. This method is called short-term harmonic analysis (Hoitink & Jay, 2016). It appears relevant to capture the seasonal variability of the constituents due to the river flow modulation (e.g., Fassoni-Andrade et al., 2023). A similar approach has been adopted in Müller et al. (2014) and Tazkia et al. (2017). This 32-day window also allows to separate Mm and MSf tidal constituents (Pugh & Woodworth, 2014), both of which have a significant amplitude along the estuary (Fassoni-Andrade et al., 2023; Gallo & Vinzon, 2005). One has to keep in mind, though, that a 32-day window is theoretically not sufficient to separate S2 and K2 tidal constituents; as a result, S2 tidal amplitude may bear some error in our analysis, typically amounting to a handful of centimeters at most over our domain of interest (Lyard et al., 2021). The part termed as "atmospheric" (hereafter ATM) is defined as the difference between the REF simulation and the NOATM simulation. The contribution termed as "discharge," noted DISCH, is defined as follows:

$$DISCH = NOATM - clim(NOATM) - TIDE$$

where *NOATM* denotes the water level from the NOATM simulation. *clim()* denotes the seasonal climatology, *TIDE* denotes the tidal part of the water level. This *DISCH* residual basically corresponds to the contribution of the river discharge, keeping in mind that all three forcings may also interact in a nonlinear way. We refrained from assessing the pure effect of the discharge, the pure effect of the tide, or the pure effect of the atmosphere, which would be obtained by model simulations forced, respectively, solely by discharge, solely by the atmosphere and solely by the tide, as they would considerably distort the realism of this dynamical modeling of the Amazon.

We remind here that our model is a 2DH version of SCHISM. As such, it does not account for the seasonal variability of the steric sea level, which amounts to 5–10 cm typically in the western equatorial Atlantic Ocean (Durand et al., 2022). Such a signal is indeed weak with regards to the signals that shall be analyzed in the present study.

Spaceborne Altimetric Water Level Records

The open-ocean tide simulated by the model was validated against the harmonic analysis of the X-TRACK along-track satellite altimetry database of Birol et al. (2017). The three tracks inside the model domain (Fig. 3) were analyzed to derive the amplitude and phase of the main tidal constituents. These validation data, whose location spans from the deep ocean to the vicinity of the Amazon mouths, are derived from the same altimetric database used to force the model sea level at its open boundaries (see "Hydrodynamical Model"). Such validation thus provides a consistent assessment of the model's ability to correctly propagate the tide over its interior domain, far from the model open boundaries and where there is no in situ data coverage.

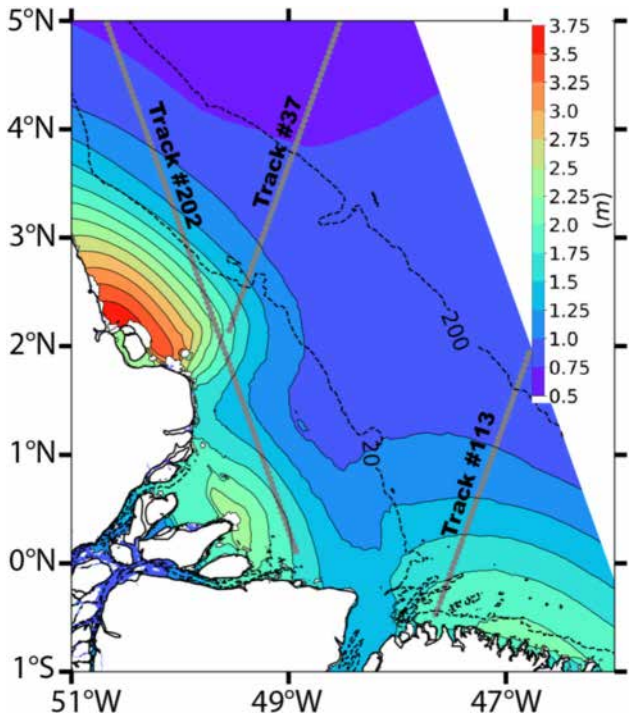

Fig. 3 Altimetric tracks considered for the validation of the open-ocean tide. The background shading represents the amplitude of the M2 tidal constituent simulated by the model. The 20-m and 200-m isobaths are displayed

In Situ Water Level Records

To validate the simulation for the tide and the yearly water level maxima simulated in the inner Amazon estuary, we considered a set of 14 tide gauge records distributed along the whole estuary (Fig. 1). Table 2 provides the details of these observational records. This dataset consists of water level observations measured typically at hourly or 10-min frequency, which is suitable for the analysis of the main tidal constituents and for the validation of water level maxima that form the focus of the present study. The period considered for tidal analyses during flood is defined as a 32-day long window during flood period for the same reasons listed in "Hydrodynamical Model," for the computation of the tidal signal from the model outputs. The same is done for the drought period. The harmonic analysis of the observed time-series was done using UTide (Codiga, 2011). Only some of the records are at least 1-year long to allow meaningful monitoring of the yearly extremes. The short records (typically one month long) were only used to infer the characteristics of the tide. For some of the observational records (in particular Escola do Igarapé Grande, which will be used in "Analysis and Validation of Modeled Water Levels"), the vertical reference of the measurements remains unknown (Fassoni-Andrade et al., 2021b).

Yearly Maximum Water Level

In the present study, a yearly maximum water level is defined as any instance of water level superior to the 99.5th percentile, computed over a year. This definition is similar to many prior studies (e.g., Haigh et al., 2010; Lyddon et al., 2018b). In practice, this means that if one considers a one-year long continuous record of hourly sea level, the events picked by our definition will consist of the 44 h of largest values recorded. Figure 4 shows the example of the water level observed in early 2017 in Porto de Santana (located 150 km upstream of the mouths, see Fig. 1). During this particular year, it is seen that the various successive maxima of water level occurred in late March and late April. The tidal signal is consistently prominent, with a very clearly defined spring-neap cycle. In this case, maxima are reached during spring tide high waters. Noteworthy, the lowest low tides of spring tide (e.g., March 30, April 29) typically lie above the lowest low tides of neap tide (e.g., April 5, May 4), which is contrary to what generally occurs in the open ocean (Pugh & Woodworth, 2014). As we mentioned in "Introduction," this feature is a characteristic of large tidal freshwater rivers (Hoitink & Jay, 2016) such as the Saint Lawrence (Matte et al., 2014) and Yangtze River (Guo et al., 2015), where the nonlinear shallow-water tidal constituents (MSf in particular) have a significant amplitude.

Table 2 Available in situ tide gauges used in the study various data sources (ANA, IBGE, Institut de Recherche pour le Développement (IRD), and data collected during this study). The relative distance corresponds to the along-river distance downstream of Óbidos (for the Amazon main course and for the North Channel of the terminal delta) and downstream of Porto de Moz (for the South Channel of the delta), in km

Station	Position	Data source	Relative distance (km)	Location	Time span	Period analyzed	
						Flood	Drought
Óbidos	55.518° W 1.918° S	ANA	0	Amazon River	08/2015–01/2020	05/2019	11/2019
Santarém	54.725° W 2.417° S	ANA	116	Amazon River	01/2000–03/2001	05/2000	11/2000
Prainha	50.481° W 1.809° S	This study	285	Amazon River	01/2020–11/2020	05/2020	10/2020
Almeirim	52.577° W 1.533° S	ANA	397	Amazon River	12/2014–05/2015; 11/2016–02/2017; 05/2018; 11/2018	05/2018	11/2018
Porto de Santana	51.167° W 0.061° S	IBGE	672	North Channel	01/2017–04/2018	05/2017	11/2017
Escola do Igarapé Grande	50.115° W 0.761° N	Brazilian Navy	827	North Channel	11/2017–05/2019	05/2018	11/2018
Ponta Guara	49.883° W 1.217° N	Brazilian Navy	892	Atlantic Ocean	04/1970–05/1970	04/1970–05/1970	
Porto de Moz	51.241° W 1.753° S	IRD	0	South Channel	04/2000–03/2001	05/2000	11/2000
Gurupá	51.651° W 1.408° S	IRD	74	South Channel	01/2000–10/2000	05/2000	09/2000–10/2000
São Pedro	51.249° W 0.940° S	This study	158	South Channel	03/2020–09/2020; 11/2021–04/2022	05/2020	11/2021–12/2021
Furo Grande de Jurupari	50.585° W 0.027° S	Brazilian Navy	292	South Channel	04/2008	04/2008	
Camarão Tuba	49.520° W 0.230° S	Brazilian Navy	355	South Channel	04/2008–05/2008	04/2008–05/2008	
Chaves	49.984° W 0.166° S	Brazilian Navy	405	South Channel	06/1966–07/1966	07/1966	
Cabo Maguari	48.416° W 0.253° S	Brazilian Navy	535	Atlantic Ocean	04/2008–05/2008	05/2008	

We assess the realism of the modeled maxima against the maxima observed at the in situ stations as follows. We start by identifying the maxima in the 400-s model outputs at the model grid point closest to the station considered. These maxima are again defined from the 99.5th percentile, computed year-wise. We then co-locate in time the modeled extreme levels with their observational counterparts, in case any valid in situ observation exists both before and after the model snapshot, within 15 min of its timestamp. This co-location in time is done through linear interpolation. A more sophisticated interpolation method could be used but would not yield significantly different results, on account of the high temporal frequency of the observed records (with in situ sampling intervals ranging from 5 to 15 min).

Tidal Calibration and Validation of the Model

We calibrated our model by adjusting regionally the Manning coefficient used to parameterize the bottom friction. REF simulation output is used to analyze and validate the tide as it includes the nonlinear interactions with the other forcings, prone to modulate the tide in our domain. This calibration was done regionally, viz. reach by reach, to match the observed tidal characteristics at the tide gauge stations (Table 2). This strategy is essentially in line with past modeling studies conducted over similarly poorly known estuarine geometries. One can quote for instance the modeling initiative of Helaire et al. (2019) dedicated to the historical Columbia River. Just like the observed records, the modeled sea level was subjected to harmonic analysis through

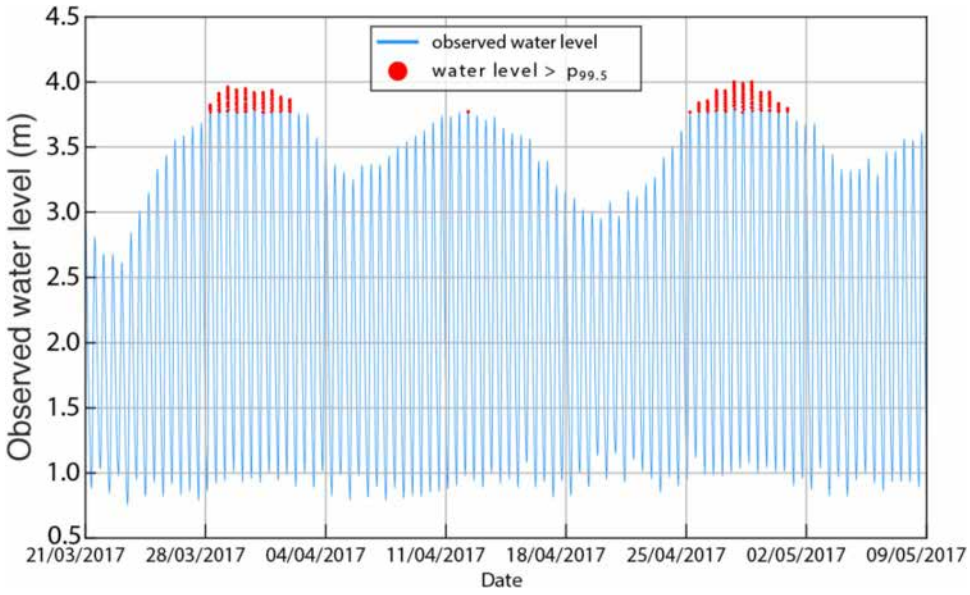

Fig. 4 Evolution of the water level observed in March to May 2017 at Porto de Santana tide gauge. The maximum water levels, defined as values above the 99.5th percentile over a given year, are displayed in red

UTide (Codiga, 2011). The realism of the model is assessed through the classical computation of the complex error (noted CE) (Andersen et al., 1995), as follows:

$$\mathrm{CE} = \frac{1}{\sqrt{2}}\left|A_m e^{i\theta_m} - A_o e^{i\theta_o}\right| \tag{1}$$

with A and θ being respectively the amplitude and the phase of a tidal constituent for (m) the model and (o) the in situ observations. This complex error simply amounts to the modulus of the complex difference between the modeled and observed tide, hereby accounting jointly for the error of amplitude and phase of the modeled tide.

For a joint assessment of the model of the five dominant tidal constituents simulated by the model, viz. M2, S2, M4, Mm, and MSf (Gallo & Vinzon, 2005), Eq. (1) translates into the following:

$$\mathrm{CE} = \sqrt{\frac{1}{2}\sum_{\mathrm{M2,\ S2,\ M4,Mm,MSf}}\left|A_m e^{i\theta_m} - A_o e^{i\theta_o}\right|^2} \tag{2}$$

Indeed, these constituents are known to be relatively important, along the Amazon estuary (Gallo & Vinzon, 2005).

Analysis and Validation of Modeled Water Levels

Oceanic Tide

The modeled M2 constituent was compared with its observed altimetric counterpart along the three tracks (Fig. 3). This constituent is the dominant one over the Amazonian oceanic shelf (Gallo & Vinzon, 2005; Le Bars et al., 2010). Figure 3 shows the spatial pattern of the dominant semi-diurnal M2 tide simulated by our REF model over the Amazonian shelf, computed using harmonic analysis from COMODO Toolbox (Allain, 2016). In line with the past studies (Beardsley et al., 1995; Le Bars et al., 2010; Ruault et al., 2020), our model reproduces a macro-tidal regime over the region, with two extended areas of M2 amplitude over of 2 m, on either side of the mouths of the Amazon around 2° N, 50.5° W, and 0.5° S, 47.5° W, and a local minimum of 0.54 m located in between them (around 1.5°

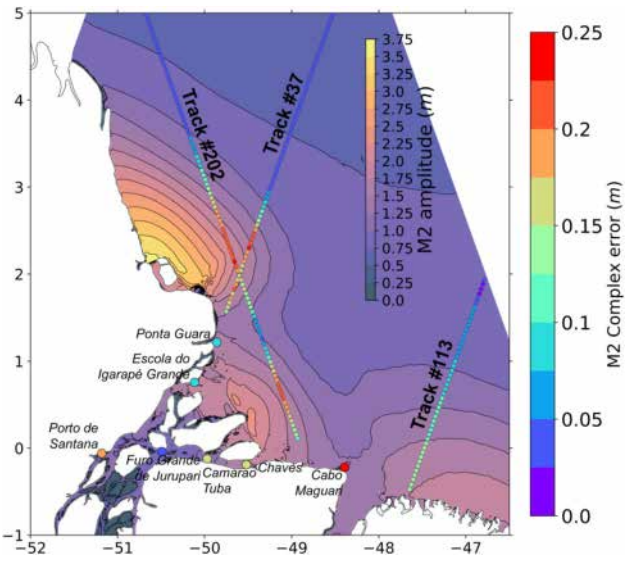

Fig. 5 Complex error of M2 simulated by the REF model along the altimetric tracks and at the coastal tide gauge stations

N, 49.5° W). Figure 5 displays the M2 complex error along the three altimetric tracks, along with the same M2 complex error at in situ stations available along the coastal ocean over the Amazon mouths. Far from the Amazon mouth and in the deep ocean (north of 3.5° N along tracks #202 and #37, and north of 1° N along track #113), the complex error typically ranges from 1 to 10 cm, viz. 10 to 50 times less than the tidal amplitude there. Closer to the coastline, this complex error gradually increases, to reach values around 0.15 m in the east region of tidal amplitude maxima on the east side of the Amazon mouths (between 0.5° S and the equator along track #113). This typically amounts to 15% of the tidal amplitude there. In the intermediate region of local minimum of tidal amplitude (between 1° N and 2° N along track #202), the complex error also reaches values of order 0.2 m. This is mostly explained by the over-estimation of the modeled tidal amplitude. At the tide gauge stations along the coastline, the M2 complex error is lower, within the range of 0.15–0.25 m. This level of performance, in line with the performance of the past published tidal models over the region (Durand et al., 2022; Gallo & Vinzon, 2005; Le Bars et al., 2010), defines the level of realism of the modeled tidal waves when they enter the Amazon estuarine system, before their subsequent propagation towards the upstream.

Estuarine Tide

Inside the Amazon estuary, the modeled tide was assessed more in-depth by comparison with the in situ tidal records (Table 2 and Fig. 1). The validation was done separately for the high-flow season (May–June) and the drought season (October–November) of the Amazon River. This is motivated by the fact that the characteristics of the tide are known to vary between these two extreme seasons in the Amazon estuary, on account of the prominent seasonality of the Amazon River discharge (Fassoni-Andrade et al., 2023; Kosuth et al., 2009).

Tide Propagation

We validated the amplitude and the phase of the main tidal constituents along the course of the estuary at the in situ tide gauges stations. Tables 6 and 7 (Online Resource 1) present the observed and modeled amplitudes and phases of the five dominant constituents (M2, S2, M4, MSf, Mm) for all stations. To gain a more synthetic view of this quantitative validation, Table 3 shows the complex errors obtained for the various stations, jointly considering all five dominant tidal constituents. The model successfully captures the observed tide, with levels of error of the same order or inferior to the error of the sole M2 constituent observed off the Amazon mouths ("Oceanic Tide"). Overall, this level of accuracy is in line with the performance of state-of-the-art tidal models in similar tropical mega-deltas (e.g., Eslami et al., 2019; Khan et al., 2020). Compared to the performance of the earlier version of our model used by Fassoni-Andrade et al. (2023), the tidal characteristics of the present model stand in significantly better agreement with the observations, throughout the estuary, both in flood season and in drought season. The reason is primarily the fine-tuning of the bottom friction coefficient we operated regionally (see "Tidal Calibration and Validation of the Model").

Tide-River Interaction

We investigated the relationship between the amplitude of the dominant tidal constituent, M2, and the Amazon discharge, sampled at monthly timescale, over the whole

Table 3 Complex error of the modeled tide (REF run) in flood season and drought season (in cm) considering the five dominant tidal constituents (M2, S2, M4, Mm, MSf). We distinguished tide gauges from the Northern Channel (NC) of and the Southern Channel (SC) of the Amazon River

Station location	Distance to ocean (km)	Complex error in flood season (cm)	Complex error in drought season (cm)
Óbidos (NC)	892	5.0	16.2
Santarém (NC)	776	4.0	15.6
Prainha (NC)	607	4.4	10.5
Almeirim (NC)	495	6.0	15.0
Porto de Santana (NC)	220	18.2	16.0
Escola do Igarapé Grande (NC)	65	14.5	9.2
Ponta Guará (NC)	0	22.3	19.4
Porto de Moz (SC)	535	8.2	10.1
Gurupá (SC)	461	9.9	10.6
São Pedro (SC)	377	5.9	8.7
Furo Grande de Jurupari (SC)	243	18.0	15.5
Camarão Tuba (SC)	180	31.7	26.8
Chaves (SC)	120	19.8	19.2
Cabo Maguari (SC)	0	36.7	37.0

2014–2018 period (for the model) and over the whole available period (for the observations) (Fig. 6). We selected three stations from the upstream part of the estuary (Almeirim) through the inner delta (Porto de Santana) to further downstream at the oceanic mouth (Escola do Igarapé Grande), to get a comprehensive view of the behavior of the estuarine continuum. In Almeirim, it is seen that M2 amplitude strongly varies as a function of the discharge, with typically five times stronger tide during the drought season (0.5–0.6 m) than during the flood season (0.1 m). This is seen similarly in the observations and the model, with a slight overestimation of the tide in the model in low discharge conditions. Expectedly, the de-tided water level lies much higher during the flood (4.5 to 5.5 m) than during the drought (2.0 to 2.5 m). The modeled de-tided water level appears biased downward by 0.3 to 0.7 m for all the discharge conditions. Further downstream, in the inner delta (Porto de Santana), a similar tide-discharge dependency can be seen in the model, though less marked: M2 amplitude decreases from 1.1 m in low discharge conditions to 1.0 m in high-discharge conditions. The available observations do not show such a trend, with M2 amplitude consistently around 1.1 m for any discharge conditions. The de-tided water level co-varies with the discharge there as well, with typically 0.2 m of increase in water level from low-discharge conditions to high-discharge conditions. The modeled de-tided water level appears biased downward, by about 0.2 m in all discharge conditions. At the mouth of the estuary (Escola do Igarapé Grande), neither the tide-discharge relationship nor the mean sea level–discharge relationship is visible in the model, with roughly constant M2 amplitude of 1.8 m, and with roughly constant de-tided sea level of 0.05 m, for all discharge conditions. The observations reveal a less consistent pattern of tidal amplitude as a function of the discharge, with values scattered around 1.6 m and 1.8 m. The observed de-tided sea level is roughly constant (slightly increasing from low discharge values to high discharge values), just like the model. Note that the absolute reference of the observations in Escola do Igarapé Grande is arbitrary (as the vertical datum is unknown there) and hence the vertical bias cannot be physically interpreted. In brief, the tide-discharge and water level–discharge relationships appear stronger in the upstream part of the estuary than at the oceanic mouth, in the observations and the model. This stands in agreement with the past observational and modeling studies of the Amazon estuary (e.g., Gallo & Vinzon, 2005; Kosuth et al., 2009; Fassoni-Andrade et al., 2023).

Estuarine Yearly Water Level Maxima

Beyond the tide, it is necessary to validate the water level maxima modeled inside the estuary, as they form the focus of the present study. We rely on the three stations of the inner estuary where we could access water level records contemporaneous with our numerical simulations. They consist of Almeirim, Porto de Santana, and Escola do Igarapé Grande, from upstream to downstream (Fig. 1). Figure 7 shows the

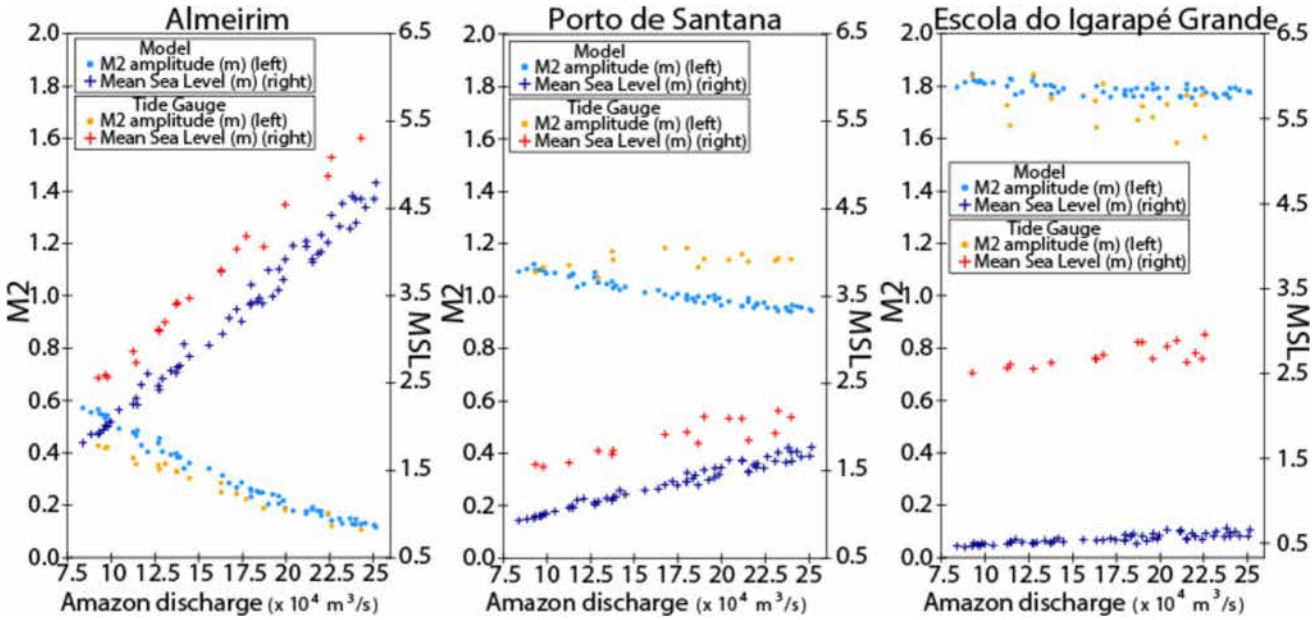

Fig. 6 Distribution of the observed and modeled amplitude of the M2 tidal constituent (bullets) and of the de-tided monthly mean water level (crosses) as a function of the Amazon discharge at Óbidos, for three stations (from left to right): Almeirim (495 km from the open ocean in the upstream estuary), Porto de Santana (in the inner delta, 220 km from the open ocean), and Escola do Igarapé Grande (at the oceanic mouth, 65 km from the open ocean). In Escola do Igarapé Grande, the vertical reference of the observed water level is arbitrary

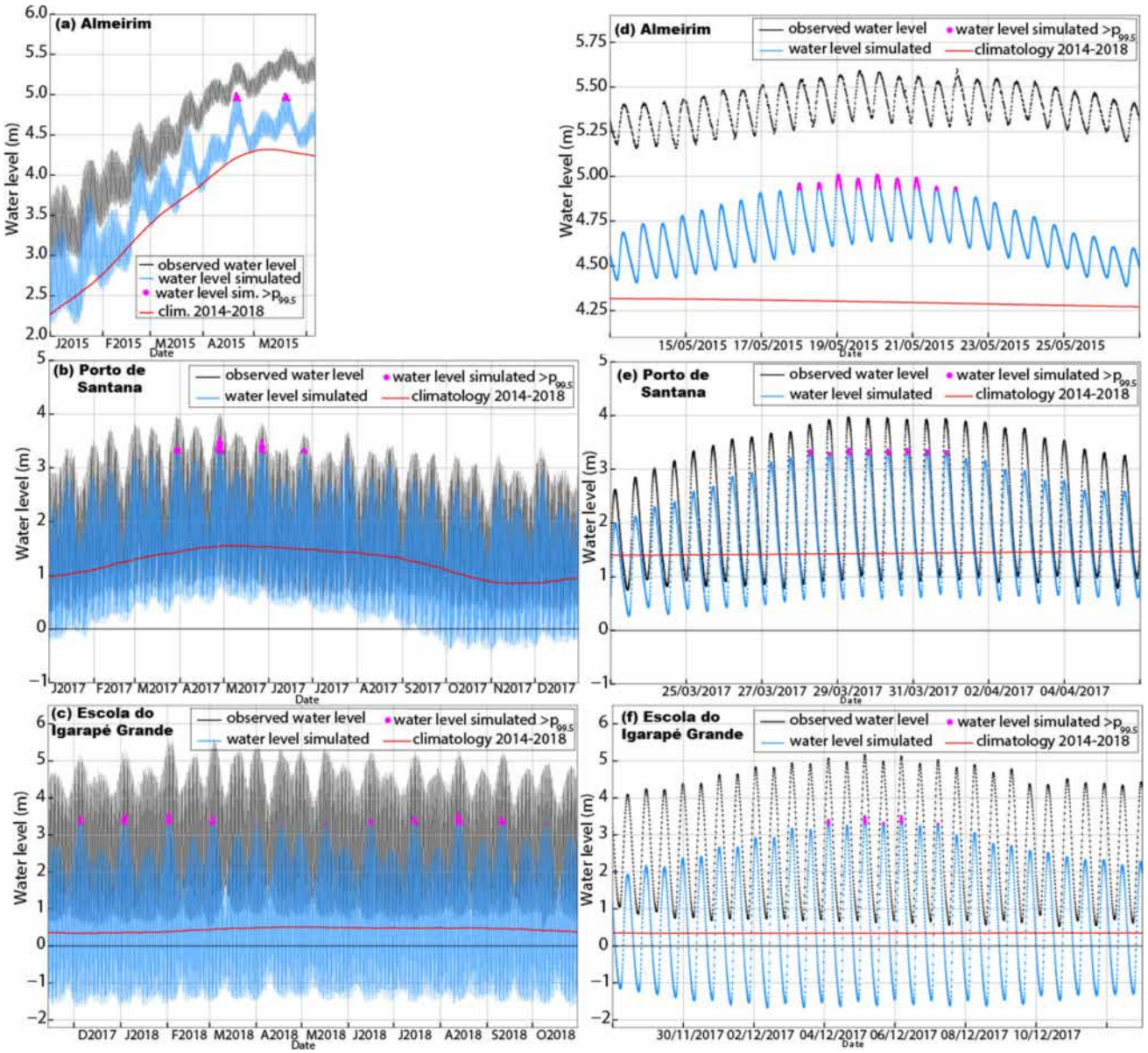

Fig. 7 Observed and modeled water level in Almeirim (**a**), Porto de Santana (**b**), and Escola Grande do Igarapé (**c**). The water level yearly maxima are displayed in pink. Panels (**d**), (**e**), and (**f**) display the same, zoomed over a particular period comprising water level maxima. The vertical reference for the observed water level in Escola do Igarapé Grande is arbitrary ((**c**) and (**f**))

observed and modeled water level during the yearly maxima events, for these stations.

In line with previous studies (Gallo & Vinzon, 2005; Kosuth et al., 2009) and consistent with what was seen in Fig. 6, the tidal imprint is ubiquitous but gradually decays from the ocean towards upstream. The spring-neap cycle is visible at all stations as a modulation of the tidal range. On top of this, in the upstream part (Almeirim, Fig. 7a), a semi-monthly tide can be seen, that results from the MSf shallow-water tidal constituent known to be strong there, typically decimetric or more (Fassoni-Andrade et al., 2023; Gallo & Vinzon, 2005). The water level maxima consistently occur around the time of high water of spring tides, for all stations (Fig. 7). Hence, they are highly intermittent in time, with typically two instances of water maximum per day.

For the model validation, we considered all years from REF run, except 2016 and 2018 as they correspond to historical deficient anomalies of the Amazon discharge throughout the flood season (Fig. 1b) with water level consistently below its climatological values (not shown), hereby making it irrelevant for our focus on extremely high-water levels. Then, we computed the model mean, the bias and the root mean square deviation (RMSD) of the modeled vs. observed yearly maximum water levels. The bias was calculated as

the mean difference between modeled and observed values during the yearly water level maximum events. The results are shown in Table 4.

The modeled water level is roughly 0.5 m too low in the inland region of the estuary during yearly maxima events (Table 4). Beyond this bias, the RMSD of the modeled water level extremes remains below 0.10 m across the domain, which is a very low value with respect to the magnitude of the water level at these stations. This is typically 30 to 50 times lower than the total value of the water level maxima (of order 3 m to 5 m), hereby evidencing the very good quality of our model. The performance of the model in capturing the water level yearly maxima appears in line with state-of-the-art modeling of water level extremes in other macro-tidal estuaries or deltas (e.g., Huang et al., 2021; Krien et al., 2017; Lyddon et al., 2018a).

Results: Mechanisms of Water Level Yearly Maximum

In this section, we investigate the mechanisms responsible for the occurrence of the water level yearly maxima using the model. We contrast the central region of the estuary (Almeirim, "Central Region of the Estuary: Almeirim"), the downstream region (Porto de Santana, "Downstream Region: Porto de Santana") and the region of the oceanic mouths (Escola do Igarapé Grande, "Oceanic Mouths: Escola do Igarapé Grande"). Here, we focus on the year 2017 only as the representative year of our 4-year-long simulations. We will generalize our analyses over the whole 2014–2018 period in the next section ("Discussion").

Central Region of the Estuary: Almeirim

Figure 8 presents the modeled evolution of the water level at Almeirim in 2017 (located roughly half-way between Óbidos and the oceanic mouths, see Fig. 1). In Fig. 8a, we present the TWL of the model and the climatology of the modeled water level computed over 2014–2018. Figure 8a also displays TIDE, the tidal component of the total water level. We computed the yearly maxima of TIDE (hereafter, TIDEmax) as well, in the same manner as for the total water level, as events above the 99.5th percentile of the yearly tidal water level timeseries. The evolution of the TWL (Fig. 8a, blue curve) shows that only one period of TWLmax occurs, at the peak of the flood season, from April 27 to May 2 (Fig. 8a, pink). The TWLmax lie between 0.65 to 0.85 m above the climatological level at that time (Fig. 8a, red curve). During TWLmax, TIDE (Fig. 8a, light green curve) does not exceed 0.4 m, much inferior to the mean TIDEmax value of 1 m that occurs much later in the seasonal cycle, during the drought season of the Amazon (October–December; dark green dots). Overall, this suggests that TIDE is not the sole driver of the yearly TWLmax in this upper part of the estuary. We investigated the specific role of the various tidal species in the TWL, in particular the semi-diurnal tide D2 (comprising M2 and S2, Fig. 8b) and the low-frequency tide (comprising MSf and Mm, Fig. 8c). This reveals that the low-frequency tidal signal (Fig. 8c) appears to dictate the occurrences of the TWLmax: although the annual maxima occur during the late April to early May period, which is not the season of maximum of the low-frequency tide (rather situated in December), they co-occur with the local maximum of this low-frequency tide, which also corresponds to spring tide in D2. This can be related with the findings of Guo et al. (2015), who discussed that in the Yangtze, in the presence of low-frequency tides of large amplitude, the level of low tide during spring tide can be higher than the level of low tide during neap tide. Here, the focus is rather on the level of high tide: in the presence of low-frequency tides of large amplitude (of order 0.25 m in the case of Almeirim), the level of high tide of spring tide D2 is much higher as if there were no low-frequency tide, so that the total water level during spring tide ends up as an extreme event. Such amplitude of the low-frequency tide is higher than the amplitude of the D2 tide.

We also assessed the role of ATM on the yearly TWLmax. Figure 8d (light blue curve) shows the evolution of ATM, as well as its seasonal climatology inferred from a 3-month running mean (black curve). One can see that the role of ATM remains weak, consistently around 0.1 m. During the episode of TWLmax, it hardly exceeds the value of its seasonal climatology. This means that ATM is not a prominent driver of TWLmax in Almeirim. Incidentally, it appears that the seasonal evolution of the atmospheric-driven water level

Table 4 Comparison between observed and modeled water levels during yearly maxima events. The model mean corresponds to the average computed across all events, with reference to the mean sea level. A positive bias means that the modeled level is above the observed one. The vertical datum of the observations is unknown in Escola do Igarapé Grande; hence, no bias can be computed there

Station location (# of validation points, and available years)	Model mean (m)	Bias (m)	RMSD (m)
Almeirim (395 pts, 2015)	4.97	−0.49	0.09
Porto de Santana (394 pts, 2017)	3.37	−0.44	0.10
Escola do Igarapé Grande (37 pts, 2017)	3.39	N/A	0.03

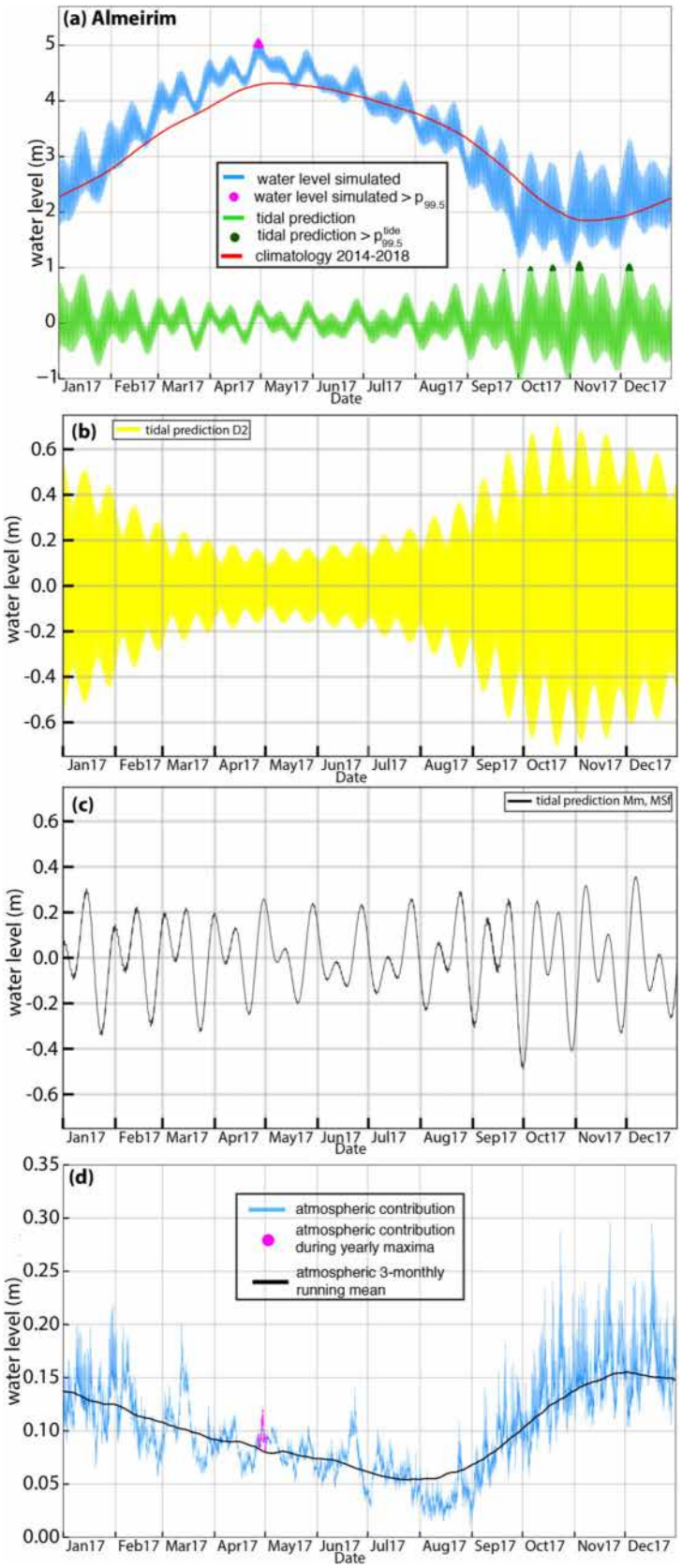

Fig. 8 Evolution of the water level simulated in the central part of the estuary in 2017, in Almeirim. **a** The blue line is the total water level simulated, with the occurrences of yearly maxima highlighted in pink. The red line is the 2014–2018 seasonal climatology. The light green curve is the tidal component of the water level simulated, inferred from a tidal prediction based on a harmonic analysis of the modeled water level. The occurrences of tidal maximum levels are highlighted in dark green. **b** The yellow line is the part of the tidal water level explained by the semi-diurnal constituents, namely M2 and S2. **c** The black line is the part of the tidal water level explained by the low-frequency constituents, namely MSf and Mm. **d** The light blue curve is the part of the water level driven by the atmospheric forcing. The pink bullets correspond to the timings of the yearly maxima of total water level shown in (**a**) in pink as well

variability is in phase opposition with the seasonal evolution of the TWL: the former reaches its maximum magnitude in the drought season (November–December), when the TWL is at its seasonal minimum. This can be explained by the fact that the wind is strongest during the season of active trade winds (Nikiema et al., 2007), which corresponds to the dry season there.

Figure 9a showcases the relative roles of the various drivers of the TWLmax in a condensed fashion. Figure 9a confirms that the yearly TWLmax consistently correspond to a high DISCH (ranging from 0.25 to 0.4 m) and TIDE (0.2 to 0.4 m), and much minor ATM (0.1 m).

Table 5 summarizes the relative contributions (in percentage) of the three forcing factors (namely the river discharge (DISCH), the tide (TIDE), and the atmosphere (ATM)) in the yearly TWLmax, obtained by averaging across all 2017 maxima. A consequence of the above definition of the three individual forcing factors is that their sum does not necessarily amount to 100%, on account of the nonlinearities among the various forcing factors (potentially non-negligible in the Amazon, see Gallo & Vinzon, 2005). In Almeirim, it appears that more than 40% of the water level maxima is accounted for by DISCH. TIDE is of the same order of magnitude, with a contribution of 46%. ATM accounts solely for hardly more than 12%. We also evaluated the relative contribution at two stations upstream of Almeirim, in Prainha (607 km from the ocean) and Santarém (776 km from the ocean). As we go further upstream, it is seen that the discharge becomes the main contributor, with DISCH up to 70% in Santarém, and TIDE gradually decays down to around 22%. The role of ATM does not vary significantly, amounting for 11.4% and 8% for Prainha and Santarém respectively.

Downstream Region: Porto de Santana

Figure 10 shows that, unlike further upstream, the occurrences of yearly TWLmax in Porto de Santana are no longer restricted to the peak flood season, as they begin to appear in early March, and disappear only in late June, which is as early as 2 months before the peak flood and until 1.5 months after it, respectively. There are five distinct periods of TWLmax, each of them separated by either 28 days or 14 days. The evolution of TIDE (green curve) clearly shows that these events, just like further upstream, coincide with high tides of spring tide. There, the tidal signal is much stronger than in Almeirim, with tidal range of order of 2 m or more, consistently all year long. Among the five spells of TWLmax, the first four ones correspond to TIDEmax events. This suggests the relative importance of the tide in triggering TWLmax there. Just like in Almeirim, we investigated the

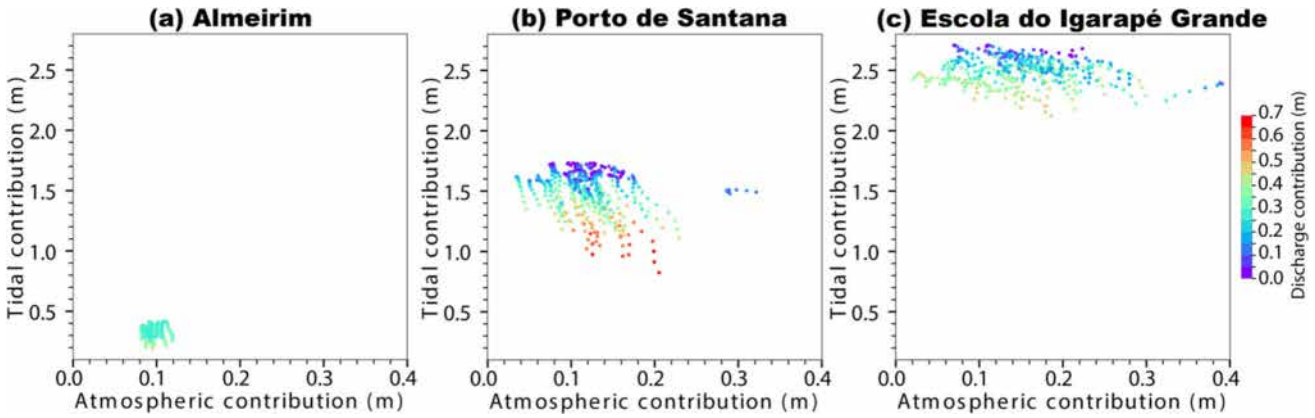

Fig. 9 Distribution of the occurrences of yearly water level maxima as a function of the atmospheric contribution (abscissa), tidal contribution (ordinate), and discharge contribution (color) for **a** Almeirim, for **b** Porto de Santana, and for **c** Escola do Igarapé Grande

Table 5 Respective roles of the various drivers of the water level yearly maxima in 2017, for the different parts of the Amazon estuary

Location	Distance to ocean (km)	Discharge forcing (DISCH)	Tidal forcing (TIDE)	Atmospheric forcing (ATM)
Very upstream estuary (Santarém)	776	70.1%	21.9%	8%
Upstream estuary (Prainha)	607	58%	30.6%	11.4%
Central estuary (Almeirim)	495	41.2%	46.1%	12.8%
Downstream region (Porto de Santana)	220	14.1%	79.3%	6.6%
Oceanic mouths (Escola do Igarapé Grande)	65	9.1%	85.6%	5.2%

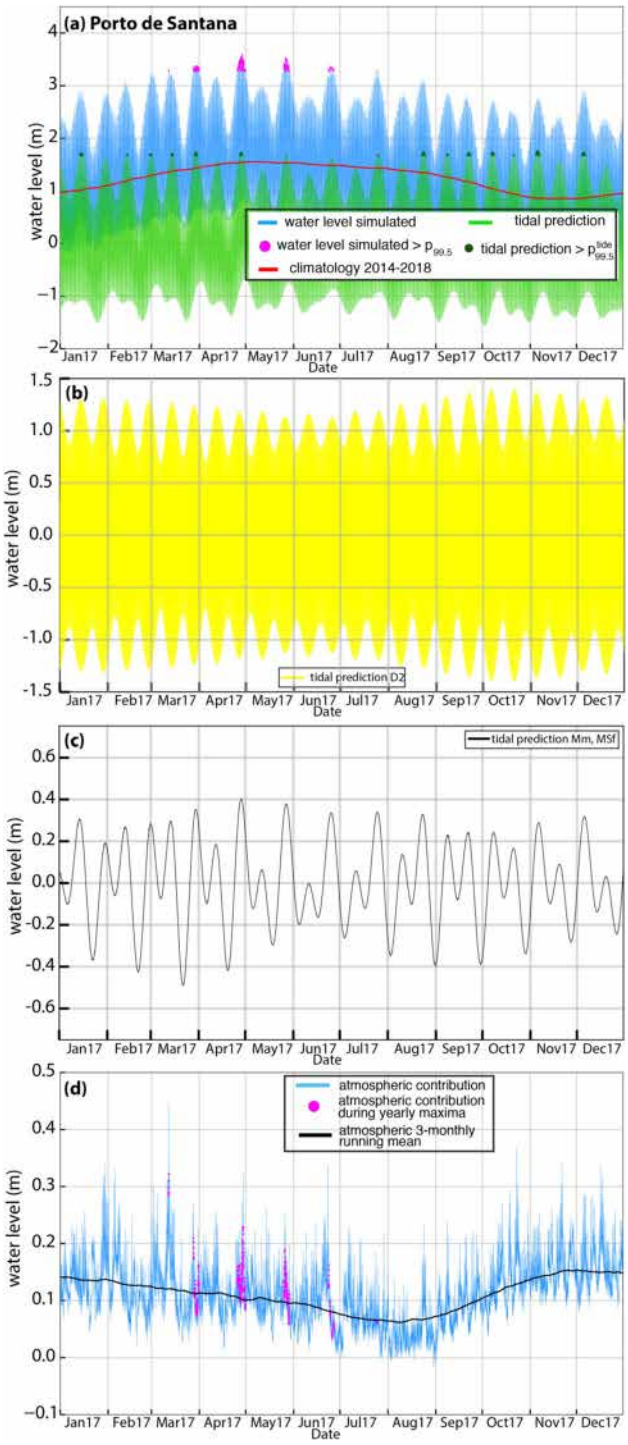

Fig. 10 Evolution of the water level simulated in 2017 in the downstream part of the estuary, in Porto de Santana. **a** The blue line is the total water level simulated, with the occurrences of yearly maxima highlighted in pink. The red line is the 2014–2018 seasonal climatology. The light green curve is the tidal component of the water level simulated, inferred from a tidal prediction based on a harmonic analysis of the modeled water level. The occurrences of tidal maximum levels are highlighted in dark green. **b** The yellow line is the part of the tidal water level explained by the semi-diurnal constituents, namely M2 and S2. **c** The black line is the part of the tidal water level explained by the low-frequency constituents, namely MSf and Mm. **d** The light blue curve is the part of the water level driven by the atmospheric forcing. The pink bullets correspond to the timings of the yearly maxima of total water level shown in (**a**) in pink as well

specific role of the various tidal species (Fig. 11bc). Here, the yearly TWLmax correspond to maxima of the low-frequency tidal signal, as well as to spring conditions of the semi-diurnal tidal signal. However, the magnitude of the low-frequency tidal water level, which ranges from 0.35 to 0.4 m, does not exceed the magnitude of the semi-diurnal tidal signal (of order 1.0 m). Still, it is commensurate with the difference between high tide of spring tide D2 and high tide of neap tide D2. In other words, thanks to the low-frequency tide, the difference between high tide of spring tide and high tide of neap tide is twice as high as if there were no low-frequency tide. This altogether contributes to the occurrence of yearly TWLmax. The fifth event of the year, at the end of June, does not specifically correspond to any TIDEmax event. However, TIDE remains high at that time, typically 20 cm below the threshold defining a TIDEmax. The two strongest TWLmax, occurring on April 28 (with a peak value of 3.59 m, that is 2.05 m above the climatology) and on May 26 (peak value of 3.52 m, that is 2.00 m above the climatology) both coincide with a significant contribution of ATM (Fig. 10d, light blue curve) of around 0.2 m. The first event of the year, on March 12, reaching 1.87 m above the climatology, although short-lived (1 h of duration) and although not the largest one (3.29 m), is associated with an even stronger ATM, exceeding 0.3 m. Across all the TWLmax, ATM is significantly superior there to what we found further upstream in Almeirim ("Central Region of the Estuary: Almeirim"). As a result, the quantification of the respective roles of the various drivers of TWLmax yields a picture more contrasted than further upstream, as seen in the statistics of Table 5: the TWLmax are dominated by TIDE (around 80%), with a relative contribution of DISCH more than three times weaker than upstream in the central estuary (14%).

Although the occurrences of TWLmax are restricted to the flood season, the striking difference between this downstream part of the estuary and further upstream in Almeirim is the propensity of both TIDE and ATM to jointly extend the duration of the season prone to water level maxima, both before and after the time of peak flood of the Amazon discharge. This results in a season prone to yearly TWLmax more than 3 months long. Figure 9b shows that, in Porto de Santana, a yearly TWLmax event occurs in the following cases:

– Either a very high TIDE (typically above 1.5 m) co-occurring with any kind of ATM (even very weak, as

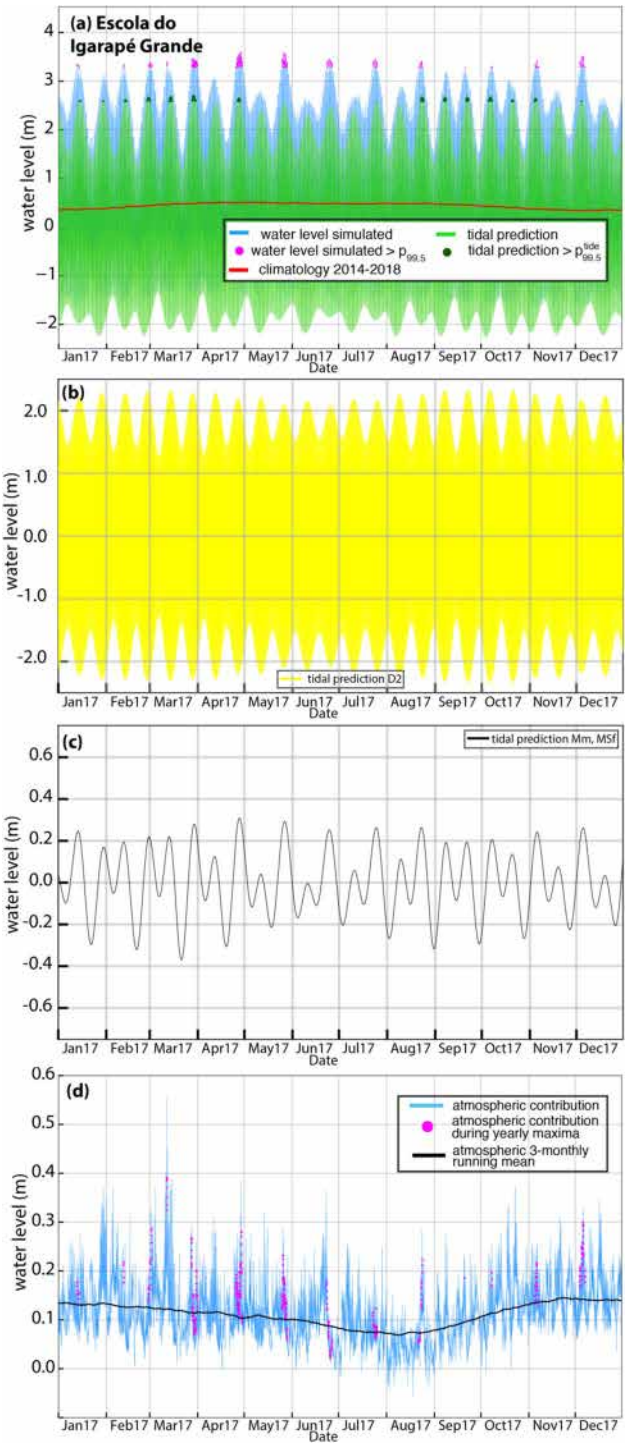

Fig. 11 Evolution of the water level simulated at the mouths of the estuary in 2017, in Escola do Igarapé Grande. **a** The blue line is the total water level simulated, with the occurrences of yearly maxima highlighted in pink. The red line is the 2014–2018 seasonal climatology. The light green curve is the tidal component of the water level simulated, inferred from a tidal prediction based on a harmonic analysis of the modeled water level. The occurrences of tidal maximum levels are highlighted in dark green. **b** The yellow line is the part of the tidal water level explained by the semi-diurnal constituents, namely M2 and S2. **c** The black line is the part of the tidal water level explained by the low-frequency constituents, namely MSf and Mm. **d** The light blue curve is the part of the water level driven by the atmospheric forcing. The pink bullets correspond to the timings of yearly maxima of total water level shown in (**a**) in pink as well

low as 2 cm) and a weak DISCH (typically inferior to 0.25 m)
- Or a moderately high tidal contribution (typically between 1.0 and 1.5 m) co-occurring with again any kind of ATM and a high DISCH (superior to 0.3 m)
- Or a high TIDE (of order 1.5 m) co-occurring with a very high ATM (around 0.3 m) and a weak DISCH (of order 0.15 m)

Oceanic Mouths: Escola do Igarapé Grande

We investigated the nature of the yearly TWLmax further downstream, near the Amazon mouths. Escola do Igarapé Grande lies on the north-western part of the mouths, right at the oceanic outlet of the North Channel (Fig. 1). Compared to the inner estuary (Porto de Santana), Fig. 11 shows that the TWL evolution is even more different here from further upstream, with TWLmax scattered all year long from mid-January to early December. Just like in Porto de Santana, TWLmax appear as highly intermittent in time, separated by either 14 days or 28 days, and consistently corresponding to high tides of spring tides. In line with past studies, it is seen that the tidal range is typically twice larger there than in the inner estuary (around 4 m; see the light green curve). With regards to the contribution of the various tidal species, a conclusion similar to Porto de Santana can be drawn: the yearly TWLmax co-occur with high tides of spring tide (for D2 species) and with high tide of the low-frequency tide. The D2 tidal signal dominates the rest; however, the amplitude of the low-frequency tide (of order 0.2 m) is of the same order of magnitude as the difference between high tide of spring tide D2 and high tide of neap tide D2 (around 0.5 m).

Like in Porto de Santana, ATM is not always strong but sometimes very significant, exceeding 0.25 m in six TWLmax instances (March 2, March 12, March 28, April 29, and December 5 or 6; Fig. 11d, light blue curve). It even exceeds 0.5 m during the March 12 event. This event is the strongest atmospheric surge seen across 2017, with a peak value of 0.56 m. Table 5 reveals that the yearly TWLmax are mostly driven by TIDE, with a contribution exceeding 85%. DISCH is even lower than in Porto de Santana, hardly reaching 9%. ATM remains modest on average, around 5%, despite the intermittent powerful surges mentioned above. Figure 9c illustrates this behavior quite distinctly from the upstream dynamics. Basically, yearly TWLmax occur:

- Either when TIDE is very high (above 2.5 m), with any kind of ATM, and any kind of DISCH

– Or when TIDE is high (between 2.1 and 2.5 m) and DISCH is high (0.3 m) to extremely high (0.5 m), irrespective of the ATM

This confirms the diversity of hydrodynamic situations conducive to yearly TWLmax in this downstream part of the estuary, with the strong contribution of any factor capable of compensating for the weak-to-moderate contribution of the other(s).

As the atmospheric surges are much stronger here than what we saw further upstream in the estuary ("Central Region of the Estuary: Almeirim"), exceeding 0.5 m in some instances, we analyzed the two model sensitivity experiments called NOWIND and NOPRESS to gain more insight on the nature of ATM. Indeed, in the other tropical estuarine and deltaic regions, it is known that the atmospheric surges are strong during storms and cyclones, and that they originate from both the wind forcing and the pressure drop associated with such low-pressure systems (e.g., Hiatt et al., 2019; Krien et al., 2017). We computed the differences between the simulations (REF minus NOWIND) and (REF minus NOPRESS), to ascertain respectively the role of the wind forcing and the role of the atmospheric pressure forcing on ATM seen on Figs. 8b, 10b, and 11b. It was found that the role of the wind forcing is completely prominent in ATM, while the role of the pressure forcing remains one order of magnitude smaller (consistently within ± 2 cm; not shown). We found that the overall temporal variability of the atmospheric pressure over the Amazon estuary has a standard deviation of about 200 Pa, which is consistent with the ± 2-cm impact on water level mentioned above under the assumption of inverse barometer response. We speculate that this weak variability may be linked to the specific location of the Amazon mouths right in the equatorial region, where the likelihood of tropical storms and cyclones is minimal (e.g., Knapp et al., 2018). Hence, we intended to focus on the structure of the wind forcing during TWLmax events. We selected the six instances of TWLmax when ATM exceeds 0.30 m at Escola do Igarapé Grande, and we computed the composite wind speed during these six events. This composite was defined as the average of the wind speed after sub-sampling it at the times of occurrence of TWLmax. As we saw in the previous section, these events are also characterized by a large atmospheric-driven anomaly of the TWL further upstream in the inner estuary in Porto de Santana, amounting typically to 90% of its value at Escola do Igarapé Grande. Figure 12 shows the spatial pattern of the wind speed composite during these extremes, as well as its average structure throughout 2017. It is seen that during TWLmax events, the wind deviates from its average West-Southwestward trade wind orientation, to blow more southwestward directly towards the bottom of the embayment where the Amazon estuary outflows. It is also seen that the wind velocity is typically 50% to 70% higher than its average value, with values around 10 $m.s^{-1}$ throughout the domain. The Amazon mouths are located right at the equator, where the Coriolis force vanishes. Hence, it is expected that such a wind pattern effectively contributes to an accumulation of

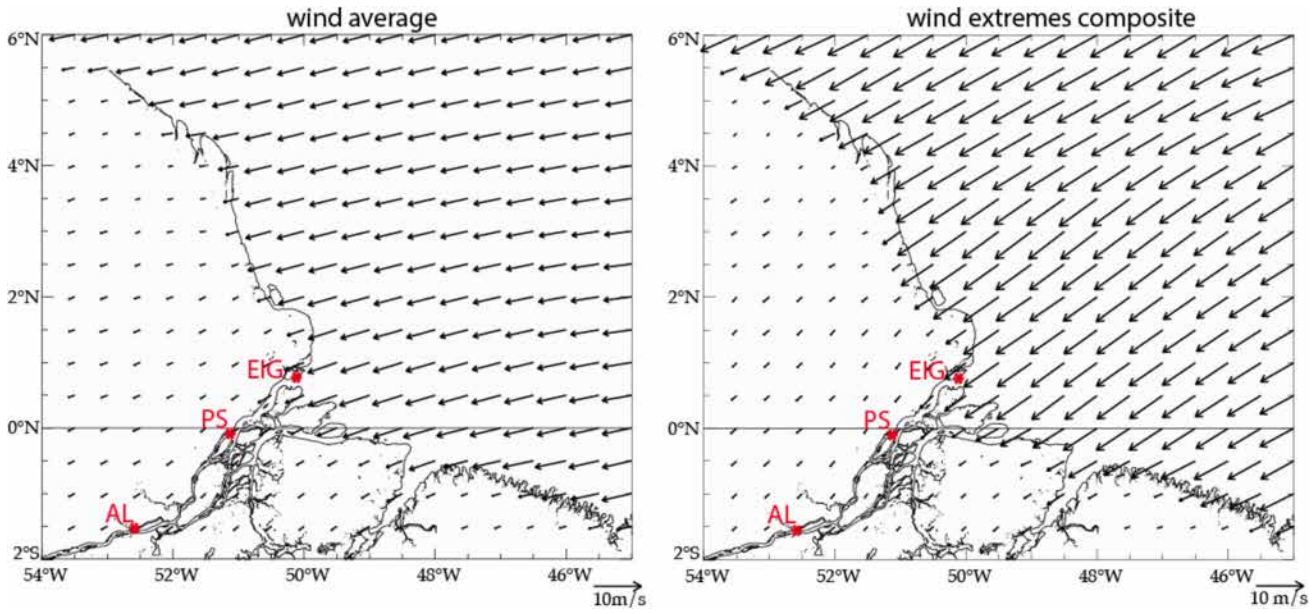

Fig. 12 Average CFSR wind speed and direction over 2017 (left) and composite during the five extreme water level events when the atmospheric contribution exceeds 0.3 m in Escola do Igarapé Grande (right). The locations of the stations are displayed in red (EIG, Escola do Igarapé Grande; PS, Porto de Santana; AL, Almeirim)

water in the coastal region in the downwind direction, viz. in the region of the mouths and further upstream in the estuary.

Discussion

Although the analyses we presented in "Results: Mechanisms of Water Level Yearly Maximum" were restricted to 2017, we verified that similar conclusions remain valid for all other years of our study period (2014–2018), with hardly any difference from year to year (not shown). We extended the quantitative assessment of the respective role of the various forcing factors on the occurrence of the yearly TWLmax to the whole 2014–2018 period, and Fig. 13 presents a synthesis of our results. We discarded the years 2016 and 2018 in our analysis, as these years correspond to a deficient Amazon discharge, when the water level remained consistently below its climatology, hereby limiting its relevance in the context of the present study. It is seen that the absolute role of the river discharge (DISCH) in the genesis of maxima (TWLmax) varies little from upstream to downstream (consistently around 0.25 m), whereas its contribution relative to the other forcing factors decreases sharply from upstream (41%) to downstream (9%). The contribution of the tide (TIDE), conversely, increases tenfold in absolute values from upstream (about 0.3 m) to downstream (over 2.5 m), with an increase in the relative part as well (from 44% upstream to 85% downstream). Interestingly, the contribution of the atmospheric forcing (ATM) also increases from upstream (0.10 m) to downstream (0.17 m), whereas its relative role decreases (from 13% to 5%). This is explained by the fact that the magnitude of the overall TWLmax with respect to the climatological level is more than four times larger downstream (over 3 m) than upstream (hardly 0.7 m). This picture reveals the complexity of the relative balance between the three forcing factors we investigated with our numerical model, across the longitudinal extent of the estuary.

TIDE globally appears as the dominant driver of the water level yearly TWLmax in the Amazon estuary. The occurrences of the TWLmax are tightly linked to the spring-neap cycle, with maxima happening during the high tides of spring tide. On account of the shallow-water nonlinear tidal constituents, and particularly the fortnightly tides (Gallo & Vinzon, 2005), during these periods of water level maxima the low tides of spring tides are higher than the low tides of neap tides. Our study shows that this peculiarity starts from Porto de Santana to further upstream (Figs. 8a and 10a). We can therefore suggest that the tidal river in the Amazon estuary begins around 220 km from the open ocean (at Porto de Santana) and extends up to around 890 km at the limit of the tidal signal in Óbidos. Compared to the other large estuaries, such as the Columbia, the Saint Lawrence, or the Yangtze (Hoitink & Jay, 2016 and references therein), this constitutes the longest tidal freshwater river. This specific feature may have detrimental impact on the propensity of the coastal areas flooded during these high-water events to get drained during the subsequent low tides.

This study highlights that the transition from a tide-dominated regime to flow-dominated regime occurs around Almeirim, 400 km from the estuary mouth. This is much further upstream than the Columbia River (100 km upstream from the mouth) (Jay et al., 2015) or the Yangtze River (245 km upstream from the mouth) (Guo et al., 2015; Shen, 2003). This may be explained by the fact that the width and depth of the Amazon estuary are both significantly superior

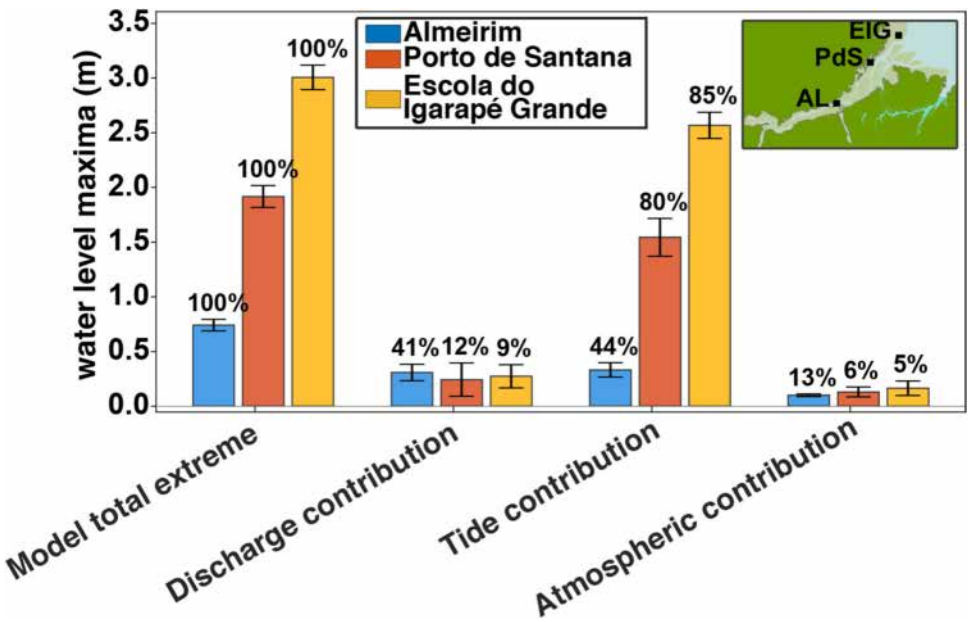

Fig. 13 Synthesis of the roles of the various forcing factors of the water level maxima along the Amazon estuary over 2014–2018. The bars show the average values (in meters) of the water level maxima with respect to the climatology, and of their three components (namely discharge-driven, tide-driven, and atmosphere-driven), with their standard deviation indicated by the vertical intervals. The percentages indicated on top show the relative contributions to the total value. The inset at the top right displays the location of the three representative sites we analyzed (Almeirim, Porto de Santana, and Escola do Igarapé Grande, from upstream to downstream respectively)

to those of the Columbia typically, hereby favoring the upstream penetration of the tidal signal. The present study provides substantiation of the along-channel gradient for the first time over the Amazon estuary.

The modeling framework we used in the present study is not without limitations. In particular, the residual errors in our modeled tidal water levels and yearly maxima water levels may improve once better knowledge of the bathymetry of the Amazon estuary and of the adjacent continental shelf become available. Although our modeling framework is based on state-of-the-art bathymetric datasets, they still suffer from large uncertainties (Fassoni-Andrade et al., 2021b). Similarly, on account of the large—though not dominant—part of the water level maxima driven by shoreward wind bursts, it would be interesting to incorporate the coupling between the hydrodynamics and the short waves in our numerical modeling framework. Indeed, in such shallow coastal regions, the water bulge of the waves setup generated during stormy weather regimes is prone to propagate towards inland over large distances in estuarine environments, hereby inducing more severe water level extremes (Fortunato et al., 2017; Khan et al., 2021). Some of the in situ tidal records we could access to validate our model date back to several decades, whereas the characteristics of the tide may have changed since then. One possible reason for long-term changes of the tide could be the geomorphic changes over the estuary, which are very poorly known in the lower Amazon. Finally, our parameterization of the bottom friction through a spatially varying Manning coefficient could also be improved, with better knowledge of the roughness of the bottom.

Conclusion

Large estuaries, located at the heart of the land-sea continuum, are a nexus of various environmental drivers of hydraulic extremes. The Amazon estuary, one of the widest estuarine regions worldwide, and the conveyor of the main fluvial discharge to the world ocean, is subject to recurrent high water level events all along its course. In the present study, we ascertained the respective roles of the three compounding drivers of the yearly TWLmax (defined as the levels exceeding the 99.5th percentile, year-wise) in the Amazon estuary, namely the river discharge (DISCH) arriving from upstream, the tide (TIDE) propagating from the adjoining ocean, and the atmospheric forcing (ATM). Our study is based on a high-resolution numerical hydrodynamic modeling framework, duly validated against extensive in situ and spaceborne observational records. We concluded that an upstream-to-downstream contrast of the typology of the TWLmax is clearly apparent, with all three drivers remaining significant throughout the estuary. We evidenced a joint prevalence of the role of DISCH and TIDE in the upstream part of the estuary, contrasting with the sole prevalence of TIDE in the region of the downstream part of the estuary and at the mouth. Besides, the gradual increase of both the tidal and atmospheric influences from upstream to downstream (in absolute values) results in a lengthening of the period prone to water level maxima from upstream to downstream: the maxima remain restricted to the immediate peak flood season upstream, whereas they occur in all seasons in the downstream part. The role of ATM on the generation of the TWLmax, although minor compared to the other two factors, increases (in absolute values) from upstream to downstream. This forcing appears related to the episodic events of shoreward anomalous wind in the region off the mouths of the estuary, conducive to an accumulation of water inside the estuary.

Relevant prospects of the present study concern the assessment of the coastal floodings induced by the TWLmax events we analyzed. Indeed, it is known that the Amazon estuary is an area of high vulnerability to the coastal floodings, with a large fraction of the riparian population exposed (Mansur et al., 2016). In the 400-km downstream-most reach of the estuary, this study highlights the importance of considering in priority the tidal variability in the occurrence of water level extremes to understand and ultimately predict the flood risk. In contrast in the upstream-most part of the estuary, upstream of Almeirim, one has to consider jointly the seasonal discharge forcing and the tide. Finally, throughout the estuary, it is important to consider the atmospheric forcing (namely the wind) as it globally increases the magnitude of the water level maxima.

The very distinct temporality of the water level maxima across the seasonal cycle, from upstream to downstream of the estuary, is of relevance for future studies of vulnerability and socio-economic risk of the riparian populations. Typically, the lengthening of the temporal window prone to floods as one moves downstream the estuary must be kept in mind when elaborating adaptation policies at regional scale.

Assessing quantitatively the spatio-temporal structure of the coastal floodings is challenging, as regards to the necessary validation of the numerical models and the paucity of observational records in this remote and densely vegetated environment (Fassoni-Andrade et al., 2021a). This may require further refinements of the modeling platforms beyond our current generation of models with horizontal resolutions of hectometric order, which remains challenging. In turn, assessing the socio-economic impacts of these recurring flooding events is necessary to mitigate the risk for the vulnerable populations in the coming years/decades.

At a time when we are certainly living the last era of the Amazon watershed in a quasi-pristine status, with countless hydropower projects already under planning (Latrubesse et al., 2017) and keeping in mind the close relationship

between peak discharge and extreme water level events over a large fraction of the Amazon estuary, the present results call for a revisit as the Amazon hydrograph gets gradually altered in the coming years.

Besides, the western Atlantic basin, just like most of the world ocean, is expected to experience a sea level rise ranging from about 0.3 m to more than 1 m by the end of the twenty-first century (Oppenheimer et al., 2019). This sea level rise can be compounded by the vertical land motions, which remain undocumented in the case of the Amazon, but which can be prominent in tropical deltas (e.g., Becker et al., 2020). This will result in trends of relative sea level that will undoubtedly profoundly impact the magnitude and dynamics of the water level extremes we analyzed in the present study, as it has been shown in other deltaic environments already (e.g., Khan et al., 2020; Khojasteh et al., 2021). Although the morphology of the estuary is bound to be altered by the end of the century, which might also impact the water level dynamics at play in the current morphology, the numerical modeling approaches such as the one implemented here provide the opportunity to investigate the future of the water level extremes.

Supplementary Information The online version contains supplementary material available at https://doi.org/10.1007/s12237-025-01483-7.

Funding Open access funding provided by Université Toulouse III - Paul Sabatier. This research has been supported by Horizon 2020 (EOSC-SYNERGY project, grant number 857647), IRD, and CNES (through a TOSCA funding). We are thankful to Marinha do Brasil, IBGE, ANA, CPRM, and SO HYBAM-IRD for the provision of the tide gauge records. Valdenira Ferreira dos Santos (IEPA) provided the Ponta Guará tide gauge data. Supercomputing facilities were provided by the HPC resources of IDRIS (France) under the project# GEN7298 granted by GENCI. This study has been partially supported through the grant EUR TESS N°ANR-18-EURE-0018 in the framework of the Programme des Investissements d'Avenir.

Data Availability All data files used in the present study will be made available by request to the corresponding author.

Declarations

Competing Interests The authors declare no competing interests.

References

Allain, D. J. (2016). TUGOm tidal toolbox. ftp://ftp.legos.obs-mip.fr/pub/ecola/tools/ttb.pdf. Accessed 15 Jan 2025

Andersen, O. B., Woodworth, P. L., & Flather, R. A. (1995). Intercomparison of recent ocean tide models. *Journal of Geophysical Research: Oceans, 100*, 25261–25282. https://doi.org/10.1029/95JC02642

Baranes, H., Dykstra, S. L., Jay, D. A., & Talke, S. A. (2023). Sea level rise and the drivers of daily water levels in the Sacramento-San Joaquin Delta. *Scientific Reports, 13*, 22454. https://doi.org/10.1038/s41598-023-49204-z

Barichivich, J., Gloor, E., Peylin, P., Brienen, R. J. W., Schöngart, J., Espinoza, J. C., & Pattnayak, K. C. (2018). Recent intensification of Amazon flooding extremes driven by strengthened Walker circulation. *Science Advances, 4*, eaat8785. https://doi.org/10.1126/sciadv.aat8785

Beardsley, R. C., Candela, J., Limeburner, R., Geyer, W. R., Lentz, S. J., Castro, B. M., Cacchione, D. A., & Carneiro, N. (1995). The M2 tide on the Amazon shelf. *Journal of Geophysical Research, 100*(C2), 2283–2319. https://doi.org/10.1029/94JC01688

Becker, M., Papa, F., Karpytchev, M., Delebecque, C., Krien, Y., Khan, J. U., Ballu, V., Durand, F., Le Cozannet, G., Islam, A. K. M. S., Calmant, S., & Shum, C. K. (2020). Water level changes, subsidence, and sea level rise in the Ganges–Brahmaputra–Meghna delta. *Proceedings of the National Academy of Sciences, 117*(4), 1867–1876. https://doi.org/10.1073/pnas.1912921117

Birol, F., Fuller, N., Lyard, F., Cancet, M., Niño, F., Delebecque, C., Fleury, S., Toublanc, F., Melet, A., Saraceno, M., & Léger, F. (2017). Coastal applications from nadir altimetry: Example of the X-TRACK regional products. *Advances in Space Research*. https://doi.org/10.1016/j.asr.2016.11.005

Callède, J., Cochonneau, Alves, F. V., Guyot, J.-L., Guimarães, V. S., & De Oliveira, E. (2010). The river amazon water contribution to the atlantic Ocean. *Revue des Sciences de L'Eau, 23*, 247–273. https://doi.org/10.7202/044688ar

Chevuturi, A., Klingaman, N. P., Rudorff, C. M., Coelho, C. A. S., & Schöngart, J. (2021). Forecasting annual maximum water level for the Negro River at Manaus. *Climate Resilience and Sustainability*. https://doi.org/10.1002/cli2.18

Codiga, D. L. (2011). Unified tidal analysis and prediction using the UTide Matlab functions. Technical Report 2011–01. Graduate School of Oceanography, University of Rhode Island, Narragansett, RI. pp. 59 https://doi.org/10.13140/RG.2.1.3761.2008

Durand, F., Piecuch, C., Becker, M., Papa, F., Sherin, V. R., Khan, J. U., & Ponte, R. (2019). Impact of continental freshwater runoff on coastal sea level. *Surveys in Geophysics*. https://doi.org/10.1007/s10712-019-09536-w

Durand, F., Testut, L., Jouanno, J., & Fassoni-Andrade, A. C. (2022). Role of the Amazon outflow on the barotropic tide on the Amazonian shelf. *Continental Shelf Research*. https://doi.org/10.1016/j.csr.2022.104695

Edmonds, D. A., Caldwell, R. L., Brondizio, E. S., & Siani, S. M. O. (2020). Coastal flooding will disproportionately impact people on river deltas. *Nature Communications, 11*, 4741. https://doi.org/10.1038/s41467-020-18531-4

Eilander, D., Couasnon, A., Ikeuchi, H., Muis, S., Yamazaki, D., Winsemius, H. C., & Ward. P. J. (2020). The effect of surge on riverine flood hazard and impact in deltas globally. *Environmental Research Letters*, *15(*104007). https://doi.org/10.1088/1748-9326/ab8ca6

Eslami, S., Hoekstra, P., Kernkamp, H., Nguyen Trung, N., Do Duc, D., Tran Quang, T., Februarianto, M., Van Dam, A., & van der Vegt, M. (2019). Flow division dynamics in the mekong delta:

Application of a 1D–2D coupled model. *Water, 11*(4), 837. https://doi.org/10.3390/w11040837

Fassoni-Andrade, A. C., Fleischmann, A. S., Papa, F., Paiva, R., Wongchuig, S., Melack, J. M., Moreira, A. A., Paris, A., Ruhoff, A., Barbosa, C., Maciel, D. A., Novo, E., Durand, F., Frappart, F., Aires, F., Abrahão, G. M., Ferreira-Ferreira, J., Espinoza, J. C., Laipelt, L., … Pellet, V. (2021a). Amazon hydrology from space: Scientific advances and future challenges. *Reviews of Geophysics*. https://doi.org/10.1029/2020RG000728

Fassoni-Andrade, A. C., Durand, F., Moreira, D., Azevedo, A., dos Santos, V. F., Funi, C., & Laraque, A. (2021b). Comprehensive bathymetry and intertidal topography of the Amazon estuary. *Earth System Science Data, 13*, 2275–2291. https://doi.org/10.5194/essd-13-2275-2021b

Fassoni-Andrade, A. C., Durand, F., Azevedo, A., Bertin, X., Guedes Santos, L., Khan, J. U., Testut, L., & Moreira, D. (2023). Seasonal to interannual variability of the tide in the Amazon estuary. *Continental Shelf Research, 255*, 104945. https://doi.org/10.1016/j.csr.2023.104945

Fortunato, A. B., Freire, P., Bertin, X., Rodrigues, M., Ferreira, J., & Liberato, M. L. R. (2017). A numerical study of the February 15, 1941 storm in the Tagus estuary. *Continental Shelf Research*. https://doi.org/10.1016/j.csr.2017.06.023

Gabioux, M., Vinzon, S. B., & Paiva, A. M. (2005). Tidal propagation over fluid mud layers on the Amazon shelf. *Continental Shelf Research, 25*, 113–125. https://doi.org/10.1016/j.csr.2004.09.001

Gallo, M. N., & Vinzon, S. B. (2005). Generation of overtides and compound tides in Amazon estuary. *Ocean Dynamics, 55*, 441–448. https://doi.org/10.1007/s10236-005-0003-8

Gévaudan, M., Durand, F., & Jouanno, J. (2022). Influence of the Amazon-Orinoco discharge interannual variability on the western tropical Atlantic salinity and temperature. *Journal of Geophysical Research: Oceans*. https://doi.org/10.1029/2022JC018495

Geyer, W. R., & Kineke, G. C. (1995). Observations of currents and water properties in the Amazon frontal zone. *Journal of Geophysical Research: Oceans, 100*, 2321–2339. https://doi.org/10.1029/94JC02657

Gibbs, J. R. (1970). Circulation in the Amazon River estuary and adjacent Atlantic Ocean. *Journal of Marine Research*, *28*(2). https://elischolar.library.yale.edu/journal_of_marine_research/1177

Godin, G. (1999). The propagation of tides up rivers with special considerations on the Upper Saint Lawrence River. *Estuarine, Coastal and Shelf Science, 48*(3), 307–324.

Guo, L., van der Wegen, M., Jay, D. A., Matte, P., Wang, Z. B., Roelvink, D. J. A., & He, Q. (2015). River-tide dynamics: Exploration of nonstationary and nonlinear tidal behavior in the Yangtze River estuary. *: Journal of Geophysical Research: Oceans, 120*, 3499–3521. https://doi.org/10.1002/2014JC010491

Haigh, I., Nicholls, R. J., & Wells, N. C. (2010). Assessing changes in extreme sea levels: Application to the English Channel, 1900–2006. *Continental Shelf Research, 30*(9), 1042–1055. https://doi.org/10.1016/j.csr.2010.02.002

Helaire, L. T., Talke, S. A., Jay, D. A., & Mahedy, D. (2019). Historical changes in Lower Columbia River and estuary floods: A numerical study. *Journal of Geophysical Research: Oceans, 124*, 7926–7946. https://doi.org/10.1029/2019JC015055

Hiatt, M., Snedden, G., Day, J. W., Rohli, R. V., Nyman, J. A., Lane, R., & Sharp, L. A. (2019). Drivers and impacts of water level fluctuations in the Mississippi River delta: Implications for delta restoration. *Estuarine, Coastal and Shelf Science, 224*, 117–137. https://doi.org/10.1016/j.ecss.2019.04.020

Hoitink, A. J. F., & Jay, D. A. (2016). Tidal river dynamics: Implications for deltas. *Reviews of Geophysics, 54*(1), 240–272. https://doi.org/10.1002/2015RG000507

Huang, W., Ye, F., Zhang, Y. J., Park, K., Du, J., Moghimi, S., Myers, E., Pe'eri, S., Calzada, J. R., Yu, H. C., Nunez, K., & Liu, Z. (2021). Compounding factors for extreme flooding around Galveston Bay during Hurricane Harvey. *Ocean Modelling, 158*, 101735. https://doi.org/10.1016/j.ocemod.2020.101735

IBGE. (2010). Instituto Brasileiro de Geografia e Estatística (Brazilian Institute of Geography and Statistics) (2010) Data from demographic census 2010. http://www.ibge.gov.br. Accessed 15 Jan 2025

Jay, D. A., Leffler, K., & Degens, S. (2011). Long-term evolution of Columbia River tides. *Journal of Waterway, Port, Coastal, and Ocean Engineering, 137*, 182–191. https://doi.org/10.1061/(ASCE)WW.1943-5460.0000082

Jay, D. A., Leffler, K., Diefenderfer, H. L., & Borde, A. B. (2015). Tidal fluvial and estuarine processes in the lower Columbia River, I. Along-channel water level variations, Pacific Ocean to Bonneville Dam. *Estuaries and Coasts, 38*, 415–433.

Khan, M. J. U., Durand, F., Testut, L., Krien, Y., & Islam, A. K. M. S. (2020). Sea level rise inducing tidal modulation along the coasts of Bengal delta. *Continental Shelf Research, 211*, 104289. https://doi.org/10.1016/j.csr.2020.104289

Khan, M. J. U., Durand, F., Bertin, X., Testut, L., Krien, Y., Islam, A. K. M. S., Pezerat, M., & Hossain, S. (2021). Towards an efficient storm surge and inundation forecasting system over the Bengal delta: Chasing the super-cyclone Amphan. *Natural Hazards and Earth Systems Sciences, 21*, 2523–2541. https://doi.org/10.5194/nhess-21-2523-2021

Khojasteh, D., Glamore, W., Heimhuber, V., & Felder, S. (2021). Sea level rise impacts on estuarine dynamics: A review. *Science of The Total Environment, 780*, 146470. https://doi.org/10.1016/j.scitotenv.2021.146470

Knapp, K. R., Diamond, H. J., Kossin, J. P., Kruk, M. C., & Schreck III, C. J. (2018). International best track archive for climate stewardship (IBTrACS) project, version 4. *NOAA National Centers for Environmental Information*. https://doi.org/10.25921/82ty-9e16. Accessed on 28/11/2022.

Kosuth, P., Callede, J., Laraque, A., Filizola, N., Guyot, J. L., Seyler, P., Fritsch, J. M., & Guimarães, V. (2009). Sea-tide effects on flows in the lower reaches of the Amazon River. *Hydrological Processes, 23*, 3141–3150. https://doi.org/10.1002/hyp.7387

Krien, Y., Testut, L., Islam, A. K. M. S., Bertin, X., Durand, F., Mayet, C., Tazkia, A. R., Becker, M., Calmant, S., Papa, F., Ballu, V., Shum, C. K., & Khan, Z. H. (2017). Towards improved storm surge models in the northern Bay of Bengal. *Continental Shelf Research, 135*, 58–73. https://doi.org/10.1016/j.csr.2017.01.014

Latrubesse, E. M., Arima, E. Y., Dunne, T., Park, E., Baker, V. R., D'Horta, F. M., Wight, C., Wittmann, F., Zuanon, J., Baker, P. A., Ribas, C. C., Norgaard, R. B., Filizola, N., Ansar, A., Flyvbjerg, B., & Stevaux, J. C. (2017). Damming the rivers of the Amazon basin. *Nature*. https://doi.org/10.1038/nature22333

Le Bars, Y., Lyard, F., Jeandel, C., & Dardengo, L. (2010). The AMANDES tidal model for the Amazon estuary and shelf. *Ocean Modelling, 31*, 132–149. https://doi.org/10.1016/j.ocemod.2009.11.001

Lyard, F. H., Allain, D. J., Cancet, M., Carrère, L., & Picot, N. (2021). FES2014 global ocean tide atlas: Design and performance. *Ocean Science, 17*, 615–649. https://doi.org/10.5194/os-17-615-2021

Lyddon, C., Brown, J. M., Leonardi, N., & Plater, A. J. (2018a). Flood hazard assessment for a hyper-tidal estuary as a function of tide-surge-morphology interaction. *Estuaries and Coasts, 41*, 1565–1586. https://doi.org/10.1007/s12237-018-0384-9

Lyddon, C., Brown, J. M., Leonardi, N., & Plater, A. J. (2018b). Uncertainty in estuarine extreme water level predictions due to surge-tide interaction. *PLoS ONE, 13*(10), e0206200. https://doi.org/10.1371/journal.pone.0206200

Mansur, A. V., Brondízio, E. S., Roy, S., Hetrick, S., Vogt, N. D., & Newton, A. (2016). An assessment of urban vulnerability in the Amazon Delta and Estuary: A multi-criterion index of

flood exposure, socio-economic conditions and infrastructure. *Sustainability Science, 11*, 625–643. https://doi.org/10.1007/s11625-016-0355-7

Matte, P., Jay, D. A., & Zaron, E. D. (2013). Adaptation of classical tidal harmonic analysis to nonstationary tides, with application to river tides. *Journal of Atmospheric and Oceanic Technology, 30*, 569–589. https://doi.org/10.1175/JTECH-D-12-00016.1

Matte, P., Secretan, Y., & Morin, J. (2014). Temporal and spatial variability of tidal-fluvial dynamics in the St. Lawrence fluvial estuary: An application of nonstationary tidal harmonic analysis. *Journal of Geophysical Research, Oceans, 119*, 5724–5744. https://doi.org/10.1002/2014JC009791

Milliman, J. D., & Farnsworth, K. L. (2011). *River discharge to the coastal ocean: A global synthesis*. Cambridge Univ. Press.

Müller, M., Cherniawsky, J. Y., Foreman, M. G. G., & Von Storch, J.-S. (2014). Seasonal variation of the M 2 tide. *Ocean Dynamics, 64*, 159–177. https://doi.org/10.1007/s10236-013-0679-0

Nikiema, O., Devenon, J. L., & Baklouti, M. (2007). Numerical modeling of the Amazon River plume. *Continental Shelf Research, 27*, 873–899. https://doi.org/10.1016/j.csr.2006.12.004

Oppenheimer, M., Glavovic, B. C., Hinkel, J., van de Wal, R., Magnan, A. K., Abd-Elgawad, A., Cai, R., Cifuentes-Jara, M., DeConto, R. M., Ghosh, T., Hay, J., Isla, F., Marzeion, B., Meyssignac, B., & Sebesvari. Z. (2019). Sea level rise and implications for low-lying islands, coasts and communities. In H.-O. Pörtner, D. C. Roberts, V. Masson-Delmotte, P. Zhai, M. Tignor, E. Poloczanska, K. Mintenbeck, A. Alegría, M. Nicolai, A. Okem, J. Petzold, B. Rama, N. M. Weyer (eds.), *IPCC Special report on the ocean and cryosphere in a changing climate*, 321–445. Cambridge, UK and New York, NY, USA: Cambridge University Press. https://doi.org/10.1017/9781009157964.006

Pugh, D., & Woodworth, P. (2014). *Sea-level science: Understanding tides, surges, tsunamis and mean sea-level changes*. Cambridge University Press. https://doi.org/10.1017/CBO9781139235778

Ruault, V., Jouanno, J., Durand, F., Chanut, J., & Benshila, R. (2020). Role of the tide on the structure of the Amazon plume: A numerical modeling approach. *Journal of Geophysical Research : Oceans, 125*(2), 1–17. https://doi.org/10.1029/2019JC015495

Saha, S., et al. (2011). updated monthly. *NCEP climate forecast system version 2 (CFSv2) selected hourly time-series products*. Research Data Archive at the National Center for Atmospheric Research, Computational and Information Systems Laboratory. https://doi.org/10.5065/D6N877VB

Sassi, M. G., Hoitink, A. J. F., de Brye, B., & Deleersnijder, E. (2012). Downstream hydraulic geometry of a tidally influenced river delta. *Journal of Geophysical Research, 117*, F04022. https://doi.org/10.1029/2012JF002448

Shen, H. T. (2003). *Saltwater intrusion in the Changjiang Estuary*. China Ocean Press.

Syvitski, J. P. M., Kettner, A. J., Overeem, I., Hutton, E. W. H., Hannon, M. T., Brakenridge, G. R., Day, J., Vörösmarty, C., Saito, Y., Giosan, L., & Nicholls, R. J. (2009). Sinking deltas due to human activities. *Nature Geoscience, 2*(10), 681–686. https://doi.org/10.1038/ngeo629

Szabo, S., Brondizio, E., Renaud, F. G., Hetrick, S., Nicholls, R. J., Matthews, Z., Tessler, Z., Tejedor, A., Sebesvari, Z., Foufoula-Georgiou, E., da Costa, S., & Dearing, J. A. (2016). Population dynamics, delta vulnerability and environmental change: Comparison of the Mekong, Ganges-Brahmaputra and Amazon delta regions. *Sustainability Science, 11*, 539–554. https://doi.org/10.1007/s11625-016-0372-6

Tazkia, A. R., Krien, Y., Durand, F., Testut, L., Islam, A. S., Papa, F., & Bertin, X. (2017). Seasonal modulation of M2 tide in the Northern Bay of Bengal. *Continental Shelf Research, 137*, 154–162. https://doi.org/10.1016/j.csr.2016.12.008

Tessler, Z. D., Vörösmarty, C. J., Grossberg, M., GladkovaAizenman, I. H., Syvitski, J. P. M. M., & Foufoula-Georgiou, E. (2015). Profiling risk and sustainability in coastal deltas of the world. *Science, 349*(80), 638–643. https://doi.org/10.1126/science.aab3574

Zhang, Y. J., Ye, F., Stanev, E. V., & Grashorn, S. (2016). Seamless cross-scale modeling with SCHISM. *Ocean Modelling, 102*, 64–81. https://doi.org/10.1016/j.ocemod.2016.05.002